NASA Contractor Report 3165

Diffusion and Phase Change Characterization by Mass Spectrometry

Mark E. Koslin and Frederick A. White

NASA

NASA Contractor Report 3165

Diffusion and Phase Change Characterization by Mass Spectrometry

Mark E. Koslin and Frederick A. White
Rensselaer Polytechnic Institute
Troy, New York

TABLE OF CONTENTS

LIST OF TABLES

LIST OF FIGURES

Part I

INTRODUCTION

The mass spectrometer has long been used as an analyt-
ical tool in many disciplines. Relative to the space program,
the mass spectrometer was one of the first major analytical
instruments to be utilized from the very inception of the
nation's program.

Virtually every major rocket was equipped with a mass
spectrometer to measure the atmosphere either on ascent or
descent and in all recent missions the mass spectrometer has
provided a wealth of information which cannot be obtained with
any other type of instrumentation. Many types of mass spec-
trometers have monitored the upper atmosphere of the earth
and are continuing to do so. Additionally, deep space probes
can be expected to continue to utilize mass spectrometry, and
the surfaces of planets are amenable to analysis by mass
spectrometry via telemetering of their chemical composition.

Another major area in which mass spectrometry has made a
contribution to NASA sponsored programs relates to the high
purity materials that have been developed for solid state
electronics. Without mass spectrometric analysis to develop
a solid state technology, the rapid advance of transistors
and other microcircuitry, computers, etc. would not have
been possible, inasmuch as the mass spectrometer has a sensi-
tivity for analyzing trace elements that generally exceeds all

other analytical methodologies.

The present work, however, relates to a more generic type of materials research that has applicability to high strength metals and alloys for advanced space vehicles, and even to the ultimate performance of composites in supersonic transports. Hence, this research represents an even further extension of the manifold applications for mass spectrometry that have occurred during the last two decades.

Specifically, this paper addresses the problem of the high temperature diffusion in metals, and it does so in a very unique manner. Until the last few years, there was rather little interest in the trace elements of metals as opposed to some of the major constituents that are generally recognized as alloying elements. However, we are now approaching an era in which the efficiency and reliability of many systems, e.g., freedom from corrosion, the attainment of theoretical yield strengths, and the macroscopic properties of materials generally are dependent upon trace metals and their transport to grain boundaries. Hence, while this present research effort is focused on a few specific materials, the technology that it utilizes should have a very broad scale application, and it is in this context that we are presenting results of a preliminary nature which will hopefully lead to an extended future study of diffusion in many engineering materials.

The first basic theory for calculating diffusion coefficients was presented by Adolf Fick in 1855.[1] Fick who modified Fourier's heat conduction equations,[2] hypothesized that in an isotropic medium the quantity of diffusing substance Q, which passes in a unit of time through a unit of transverse cross sectional area, is proportional to the concentration gradient measured along the normal to the section:

$$Q = -D(dC/dx) \quad . \tag{1}$$

The above equation is called Fick's first law for equilibrium flow, C is the concentration of the diffusion substance in units of mass/cm^3, x is the spatial coordinate in units of cm., and D is the diffusion coefficient with units of cm^2/sec. In the case of non-equilibrium flow, Fick's second law can be derived from the first law by considering the rate of accumulation of the diffusing substance in a given element of volume as the difference between the incoming and outgoing fluxes per unit time. This yields

$$\frac{dC}{dt} = D \frac{d^2C}{dx^2} + D \frac{d^2C}{dy^2} + D \frac{d^2C}{dz^2} \tag{2}$$

Fick's laws were shown to be approximations to more general transport equations, and they may apply only to several atomic distances from solute sources or sinks, when the solvent is a homogeneous medium and when the solute concentrations are small.[3] Boltzmann extended the application of Fick's equations to large solute concentrations,[4] and these modified equations were graphically solved by Matano[5] in 1936 for metallic

3

diffusion. To date, experimental determinations of the diffusion coefficient have always followed a prescribed procedure. The solute material was allowed to diffuse at a known temperature and for a known time into a block of solvent material of such a shape that Fick's laws yielded an exact mathematical solution for the diffusion process in the system. Next, the solute concentration was measured at known points throughout the solvent. These values of solute concentration, and the diffusion coefficient was found algebraically or graphically. The problem of experimentally determining the diffusion coefficient thus became one of accurately determining the solute concentrations throughout the solvent, and of fulfilling the initial and boundary conditions applicable to a particular form of Fick's laws.

The methods which various experimenters have used to determine the solute concentrations and to satisfy the Fick's law boundary conditions in their experiments are quite diverse. An excellent summary of these different methods have been compiled by Gertsriken and Dekhtyar.[6]

The introduction of radioisotopes in the 1940's enabled the concentration of a radioactive solute in a solvent specimen to be determined quite readily by nuclear radiation detectors. It is now advantageous to illustrate these standard methods.

Serial Sectioning: This method involving radioactive tracers is most frequently used in the study of diffusion. The sample after being held at a given temperature for a known amount of time (annealing time) to allow the radioactive tracer to diffuse into the sample, is subjected to a series of sectioning

operations. The sample is weighed before and after each cut to determine the thickness of the material removed. The cuttings are collected and their activity measured with a Geiger or scintillation counter. From the weights and the density, the coordinates of the midpoints of each slice, (x), are calculated. A plot of the natural logarithm of the activity versus x^2 has a slope of $-1/4Dt$ for volume diffusion. Hence, if the time of the anneal, t, is known, the diffusion coefficient D may be calculated.

The main advantage of the serial sectioning method is that it is simple, direct, and doesn't depend on the properties of the radiation from the radioactive material used, assuming no damage to substrate by ionizing radiation from the radio-isotope.

Residual Activity Method: This method is similar to the serial sectioning analysis in that layers of thickness x are removed, but the total remaining activity, I, of the sample is measured in this case.

In the case of weakly absorbed radiation (strong gamma rays) a plot of $\ln(-dI/dx)$ versus x^2 should be a straight line of slope $-1/4Dt$; and in the case of strongly absorbed radiation (weak beta-rays) a plot of $\ln(I)$ versus x^2 should also be a straight line of slope $-1/4Dt$.

Surface Decrease Method: In this method, the total activity of the specimen is measured as a function of time. No sectioning of the sample is necessary.

5

Autoradiography: The principle of this method is to determine
the photographic density of the blackening of an exposed
emulsion as a function of the distance from the interface of
the specimen with the initial radioactive deposit. The speci-
men is usually cut at a measured angle α (usually 90°) to the
initial face, and the cut face is placed in contact with a
piece of appropriate X-ray film. The blackening of the emulsion
(which is usually found to be directly proportional to the
cconcentration of activity) is measured with a micro-densitom-
eter. A plot of ln (photographic density) versus x^2 has a slope
of -1/4Dt from which D may be calculated if the anneal time,
t, is known. This method offered two distinct advantages; 1)
since the filament was small, the times involved in heating
and cooling it were small, and 2) because of the source mount-
ing and the high vacua of the mass spectrometer the diffusing
system was negligibly affected by any reaction between it and
the surrounding environment at the experimental operating
temperatures.

With the advent of sophisticated electronics, new devices
have been developed for studying solid state phenomena. The
electron-beam microprobe is one of the most important as far
as diffusion studies are concerned. The device collimates a
beam of electrons into a 1 μ diameter "pencil" which is
directed onto the specimen surface at the spot to be analyzed.
The electron bombardment causes characteristic X-rays to be
mitted from the sample. These X-rays are then detected and
analyzed to determine composition of the bombarded surface.

The limit of detectability is about 10^{-14} grams for elements of high atomic number.[7]

Existing procedures and techniques used for material characterization are adequate for materials which are to be operated in a normal temperature environment. However, at elevated temperatures (above 800°C), there is a need for improved measuring techniques. It is very important to understand the effects of high temperature operation on the materials, i.e., to determine whether or not the elevated temperature will cause matter from the environment to be absorbed into the material and then be transported through it, or whether some constituent of the material will be removed. The transport of constituents either into or out of the material can change the structural integrity of the material. As the high temperatures diffusing system tends to react with its environment. Also rapidly heating and cooling of the solute-solvent system will often adversely affect the diffusion measurements. In 1960, McCracken and Love[8] developed a system for determining diffusion coefficients utilizing a mass spectrometer, and a thermal ionization source.

Using a mass spectrometer with a thermal ionization source, only solute atoms of a single isotope would be observed, and diffusion rates in a specified temperature range could be obtained. The assumption is made that Fick's solution for one dimensional diffusion in an outgasing thin plate can be applied. The solute ion current out of the filament as a function of time is thus:

7

$$J_{ion} = A \exp \left(-\pi^2 Dt/x^2\right) \tag{3}$$

where A is a constant of proportionality, D is the diffusion coefficient, x is the filament thickness, and t is the measurement time. Hence, the slope of a plot of the natural logarithm of the solute ion current versus time will yield the desired diffusion coefficient, provided the thickness of the filament is known.[9]

General Advantages of the Mass Spectrometric Technique: There were many reasons for choosing the mass spectrometric approach for determining diffusion characteristics. As the mass spectrometer analyzes one mass at a time, there is no ambiguity caused by interfering masses. Since the filament is small, the times involved in heating and cooling it are also small. The probability of a reaction occuring between the high temperature specimen and the surrounding environment is negligible due to the mounting and the high vacua of the mass spectrometer. Finally, the sensitivity of the instrument permits the impurity level to be less than a part per billion, thus no doping of the sample is necessary and commercial grade material can be utilized.

Importance of Sample Materials: The materials studied in this work were tantalum, zircaloy-2, and 304 stainless steel. These materials were chosen for two basic reasons. First, they represent a family of materials which go from being ultra pure (99.996% Ta) to a 1.5% alloy with zirconium, to a 70% Fe,

18.5% Cr, 9% Ni, alloy (304 stainless steel). Hopefully, this will enable one to draw conclusions about diffusion rates in alloys rather than ultra-pure single crystals. Secondly, these materials are of current interest to the nuclear industry where higher operating temperatures mean higher efficiencies.

The alkali metals were chosen as the elements of interest primarily due to their relatively low ionization potential (making them more suitable for thermal ionization) and due to the fact that they probably appear in most materials as naturally occurring impurities - thus eliminating doping of the host matrix. It was decided that concentrating these experiments on an entire chemical family might yield an overall diffusion mechanism which would allow diffusion rates of other impurities and sample materials to be approximated.

Use of trade names or names of manufacturers in this report does not constitute official endorsement of such products or manufacturers, either expressed or implied, by the National Aeronautics and Space Administration.

Part II

ATOMIC DIFFUSION THEORY

A. General Considerations

Diffusion is one of the mechanism by which matter
is transported through matter. From the theory of specific
heats, it is known that atoms in a crystal oscillate around
their equilibrium position. Occasionally these oscillations
become large enough to allow an atom to change sites. The
net result of many such random movements of a large number of
atoms is actual displacement of matter, the movement being
activated by the thermal energy of the crystal.[10] The path
of an individual particle is an unpredictable zigzag. The
length of an individual step in this zigzag is determined
in a solid by its jump length, b, i.e., the distance the
particle is able to move when it acquires enough energy to
make one jump.

The frequency of jumping, f, is the vibrational
frequency multiplied by the probability that the vibrating
atom has the activation energy to make the jump;

$$f = (1/3)\omega \exp (G_D/RT) \tag{4}$$

where ω is the vibrational frequency, 1/3 allows roughly for
the fact that only about 1/3 of the randomly directed vibra-
tions are in the required direction, and G_D is the free
energy of activation.[11] From this we can obtain an equation
for the diffusion coefficient, D,

$$D = (1/2) \ b^2 f \tag{5}$$

B. Diffusion Mechanisms

How the substance diffuses through the material is just as important as the diffusion coefficient formula itself. There are quite a variety of mechanisms by which an atom can move from one position to another in a crystalline structure.

Vacancy Mechanism: In all other than perfect crystals, some of the lattice sites are unoccupied. These unoccupied sites are called vacancies. If one of the atoms on an adjacent site jumps into the vacancy, the atom is said to have diffused by a vacancy mechanism, see Figure 1(b).

Interstitial Mechanism: When small atoms dissolve in metallic lattices as impurities so as to occupy interstitial positions between solvent atoms and an atom passes from one interstitial site to one of its nearest neighbor interstitial sites without permanently displacing any of the matrix atoms an interstitial mechanism is said to have taken place. The interstitial mechanism is thought to operate in alloys for those solute atoms which normally occupy interstitial positions. It will be dominant in any nonmetallic solid in which the diffusing interstitial doesn't distort the lattice too much,[12] see Figure 1 (a).

Interchange or Exchange Mechanism: This is the direct exchange of two nearest neighbor atoms.

Ring Mechanism: A more general form of the exchange mechanism consisting of a number (three or more) of

11

| a | b |
| Interstitial Mechanism | Vacancy Mechanism |

| c | d |
| Interstitiality Mechanism | Crowdion Mechanism |
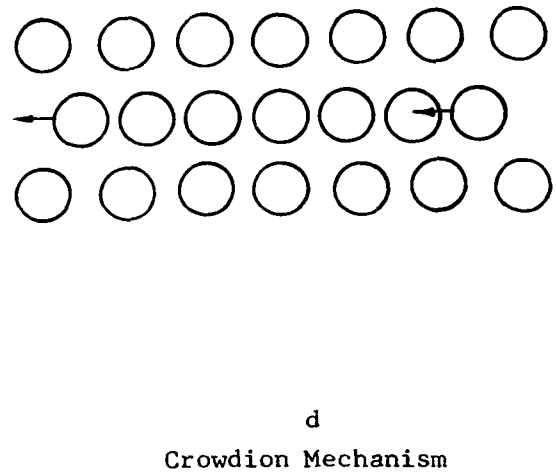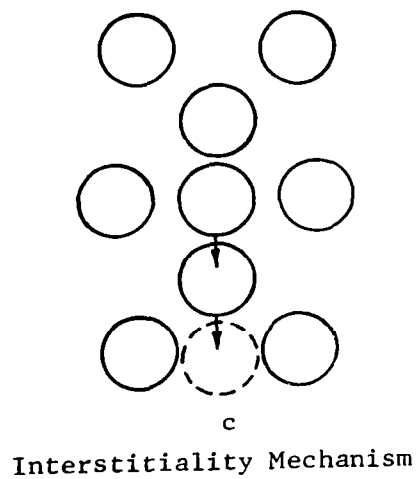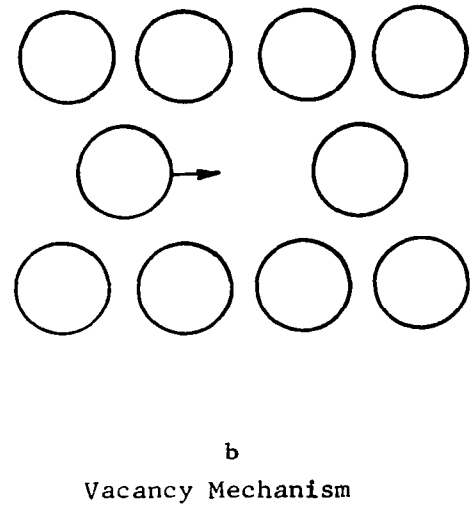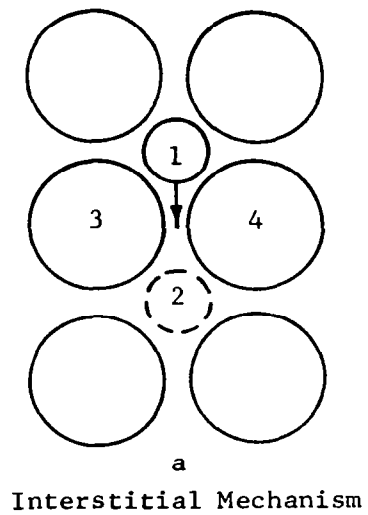
DIFFUSION MECHANISMS

Figure 1

12

atoms forming a closed ring. Atomic diffusion then takes place by rotation of the ring.

Interstitialcy Mechanism: An interstitial atom moves from an interstitial site to an adjacent normal lattice site displacing the atom that had occupied that site into a new interstitial site, see Figure 1 (c).

Crowdion Mechanism: A line imperfection consisting of n nearest neighbor atoms compressed into a space normally occupied by (n-1) atoms. Diffusion then takes place by movement along the line of atoms, see Figure 1 (d).

Dislocation Mechanism: Dislocations can provide easier paths for diffusion than a perfect lattice. The diffusion of dislocated atoms can be produced in two ways: 1) the diffusion of the dislocated atoms over the interstices and 2) displacement of the dislocated atom from the interstice into a normal site of the lattice, and the atom situated in the lattice goes over into the interstice.

C. Theoretical Methods of Diffusion Coefficient Calculations

While the mechanisms of diffusion may be summarized from purely qualitative consideration, the problems involved in quantitatively calculating a diffusion coefficient for a specific solute-solvent system are quite complex. A convenient first step towards solving these problems is the consideration of the rate at which the solvent atoms themselves move around in the solvent lattice, or the self-diffusion coefficient of the solvent material. After a solution

has been found to the problem of self-diffusion, the effects of a solute impurity are treated as a superposition problem. The relationship between impurity diffusion coefficient and the self-diffusion coefficient is discussed in section C-2.

C-1   Self-Diffusion

Introduction: In a pure metal, diffusion operates by the vacancy mechanism and the self-diffusion coefficient is determined by the frequency with which an atom will jump into a vacant neighboring site, ω, and by the probability that a given neighboring site is vacant, P_v. These experiments are usually performed by plating a very thin film of radioactive tracer on a pure metal, annealing, sectioning, and using the thin film solution to determine D_s.[13] This D_s is called the self-diffusion coefficient of the solute in the given solvent, and the experiments are done ideally at "infinite dilution." For the infinitely dilute alloy, the problem is then to estimate whether and by how much ω and P_v for a solute atom differs from ω and P_v for a solvent atom.

C-1.1   Mathematical Model: A general approach to the derivation of the diffusion coefficient is to consider the problem as a whole sequence of jumps that result in paths of atoms migrating through the lattice rather than merely jumps between two planes. This concept is referred to as the "random walk" approach.

Consider that successive atom jumps are vectors $\bar{r}_1$, $\bar{r}_2$, etc. If Γ is the total number of completed jumps which an atom makes per unit time, then after a time t, a total of n = tΓ completed jumps will have occurred, and the atom will have moved an average distance, $\overline{R(t)}$

$$\overline{R(t)} = \Sigma \bar{r}_i \tag{6}$$

from its initial position. It may be shown that the diffusion coefficient, D, is obtained by

$$D = \overline{R(t)}^2/6t \tag{7}$$

where

$$\overline{R(t)}^2 = |\bar{R}(t) \cdot \bar{R}(t)| .$$

Now

$$\overline{R(t)}^2 = \Sigma\overline{(r_i)}^2$$
$$= \bar{r}_i^2 + 2\Sigma\Sigma r_i \cdot r_{i+j} . \tag{8}$$

For the case of the fcc, bcc, and hcp crystal systems, all the jump vectors will be of equal magnitude, r. Then equation (8) may be written as

$$\overline{R(t)}^2 = nr^2 + 2r^2\Sigma(n-j)\overline{\cos\theta_j} \tag{9}$$

where $\overline{\cos\theta_j}$ is the average value of the cosine of the angle between the ith and the $(i+j)^{th}$ atom jump.

If the direction of each jump is independent of all earlier jumps, then $\overline{\cos\theta_j} = 0$ and substituting equation (9) into equation (7) we obtain

$$D = (1/6)\Gamma r^2 . \tag{10}$$

The factor (1/6) come from the fact that only 1/3 of the randomly directed vibrations are in the required direction, and then substituted into equation (5).

As an example, consider an fcc lattice. For this case Γ = 12ωN, where 12 is the number of nearest neighbors, ω is the jump frequency, and N_v is the fraction of vacant sites. With a lattice constant a_o, for vacancy diffusion

$$D = a_o^2 \, N_v \omega \quad ,$$

while for interstitial diffusion

$$D = \delta a_o^2 \omega$$

with δ being a geometric constant. [14]

The problem of determining D has now been reduced to finding a way of calculating N_v and ω .

C-1.2   <u>Correlation Effects</u>: The assumption of uncorrelated motion made in the derivation of equation (9) is valid for interstitial diffusion in dilute alloys. However, it is not valid in the case of vacancy or interstitialcy diffusion. Consider vacancy diffusion, after an exchange between an impurity atom and a vacancy all of its neighbors are not identical; one of them consists of a vacancy, it is most probable that the impurity atom will jump back to the position occupied by the vacancy. In other words, the mean square displacement for the impurity atom after n jumps, $\overline{R}_i^2$, will be less than that for a vacancy which took the same number of jumps, $\overline{R}_v^2 = nr^2$. The ratio of these two quantities defines the correlation factor, f, as

$$f = \lim_{n \to \infty} \overline{R}_i^2 / \overline{R}_v^2 \quad . \tag{11}$$

16

The correlation factor has been calculated by
Compaan and Haven.[15] They demonstrated that the correlation
factor could be written as

$$f = \overline{1 + \cos \theta_i} / 1 \overline{- \cos \theta_i} \qquad (12)$$

where $\overline{\cos \theta_i}$ refers to the average of the cosine of the
angle between consecutive jumps. For vacancy diffusion in
a fcc lattice, where the terms have been previously defined,

$$D = a_o^2 f \omega N_v \quad .$$

C-1.3   Calculation of N_v: According to classical ther-
modynamics, a given system tends to assume a configuration
such that the free energy of the system is a minimum. This
free energy G is related to the enthalpy, H, temperature in
degrees Kelvin, T, and entropy, S, of the system by

$$G = H - TS \qquad (13)$$

The entropy of any system may be divided into two
parts, the thermal entropy S_t and the configurational
entropy S_c. The thermal entropy S_t is determined by the
number of different ways W_t in which the thermal energy of
the crystal may be distributed over the possible vibrational
modes of the individual atoms. W_t is related to S_t by the
Boltzmann relation, where k is Boltzmann's constant,

$$S_t = k \ln W_t \quad . \qquad (14)$$

The configurational entropy of a crystal S_c is determined by
the number of different ways W_c in which the atoms of the

crystal may be arranged over the available number of lattice sites. For the case of vacancies in a crystal, let N_a be the number of atoms in the crystal and n_v be the number of vacancies, and let all of the lattice sites be equivalent. It can be then shown that this case[16]

$$W_c = \frac{(N_a + n_v)!}{(N_a! \; n_v!)} \quad . \tag{15}$$

Again the relation between S_c and W_c is given by the Boltzmann relation

$$S_c = k \ln W_c = k \ln \frac{(N_a + n_v)!}{(N_a! \; n_v!)} \quad . \tag{16}$$

Now assume the energy to create a vacancy in a crystal to be h_v. The enthalpy of a single crystal containing n_v vacancies is increased by a factor $n_v h_v$ over that of a perfect crystal. For reasons given below, the thermal entropy will increase by a factor $n_v \Delta s_t$ when n_v vacancies are added to the crystal. Thus, from these considerations and from equations (13) and (16), the free energy of an imperfect crystal as a function of n_v and T becomes,

$$G(n,T) = G_{perfect}(T) + n_v h_v - n_v T \Delta s_t - k \ln \frac{(N_a + n_v)!}{(N_a! \; n_v!)} \tag{17}$$

In order to find the equilibrium value of n_v, we note that at equilibrium $\partial G / \partial n_v = 0$. Using this fact, and the approximation that $\ln x! = x \ln x$ for $x < 1$, we have from (17)[17]

Note: Lower case letters indicate a property of a single crystal, while a capital letter indicates a property of an entire crystalline structure.

18

$$\frac{n_v}{n_v + N_a}\bigg|_{eq} = \frac{n_v}{N_a}\bigg|_{eq} = \exp\frac{\Delta S_t}{k} \exp\frac{-h_v}{kT} \quad . \quad (18)$$

Here, $(n_v/N_a)_{eq}$ is the equilibrium atomic fraction of vacancies in the crystal. In terms of the equilibrium mole fraction of vacancies N_v, equation (18) may be written

$$N_v = \exp\frac{\Delta S_t}{R} \exp\frac{-H_v}{RT} \quad . \quad (19)$$

In equation (19), ΔS_t and H_v refer to the thermal entropy and enthalpy changes of the entire crystal due to the addition of N_v vacancies.

It should be noted that the foregoing derivation assumed that s_t and h_v are independent of n_v/N_a, which would be true if n_v/N_a, or N_v, were very small. Experimentally, N_v has been found to be about 10^{-4} in pure metals,[18] so this assumption is a reasonable one.

The enthalpy of a crystal should change with the addition of a vacancy, and this energy change equals approximately the energy necessary to remove an atom from the interior of the crystal and place it on the crystal surface. The reason for the change in S_t, however, is more subtle. One way to estimate this change is to assume an Einstein model for the solid consisting of N atoms equally distributed over 3N harmonic oscillators.[19] When ν is the Einstein frequency of the atoms in a perfect crystal and $h\nu \ll k$, where h is Plank'sconstant, and k is Boltzmann's constant, then S_t, the thermal entropy can be shown to be [20]

19

$$S_t = 3N_a k \left| 1 + \ln \frac{kT}{h\nu} \right| \qquad (20)$$

for that perfect crystal. In a crystal containing n_v

the atoms around a vacancy will have a vibrational frequency ν' less than ν because the atomic restoring forces are reduced. Again using the Einstein model, each atom neighboring a vacancy is assumed equivalent to 3 harmonic oscillators of frequency ν' . For N_a atoms and n_v vacancies in a crystal, we have

$3n_v x$ oscillators of frequency ν

$(3N_a - 3n_v x)$ oscillators of frequency ν'

where x is the number of nearest neighbor atoms around each vacancy. Applying this to equation (20), we have that the thermal entropy of an imperfect crystal is:

$$S_t = 3n_v x k \left| 1 + \ln \frac{kT}{h\nu} \right| + (3N_a - 3n_v x) k \left| 1 + \ln \frac{kT}{h\nu'} \right|$$

$$(21)$$

The change in thermal entropy due to the addition of n_v vacancies to a perfect crystal can be estimated by subtracting (20) from (21) and dividing by n_v to obtain

$$S_t = 3xk \ln (\nu/\nu') \qquad . \qquad (22)$$

Thus the change in thermal entropy is due primarily to the change in vibrational frequency of the atoms around the vacancies.

20

Calculation of ω: While the calculation of N_v is a
straightforward one, accurate determination of the atomic
jump frequency for a tracer atom is quite difficult. In
fact, the accuracy of the present calculations of ω is so
poor that such calculations provide no real verification of
experimentally determined diffusion coefficients. However,
the following relatively simple theoretical treatment of
ω yields a numerical value of this parameter within at
least an order of magnitude, and it further provides some
insight into the temperature dependence of this quantity.

First, assume a simplified sequence of atomic motions
required for a tracer atom to jump from one lattice site
to another, as shown in sequence Figures 2a, 2b, and 2c.
Before such a sequence can occur, the tracer atom must
attempt a jump in the direction of the vacant site, with
the two restraining atoms simultaneously moving far enough
apart to let the tracer atom slide between them. The
atomic configuration shown in Figure 2b is called an
activated complex, and consists of a region containing a
diffusing atom between two equilibrium sites. The number
of atoms diffusing per second in one mole of solvent
material equals the mole fraction of activated complexes
N_m, multiplied by the average velocity of the diffusion atoms
moving between the restraining atoms $\bar{v}$, divided by the
width of the barrier created by these restraining atoms δ.
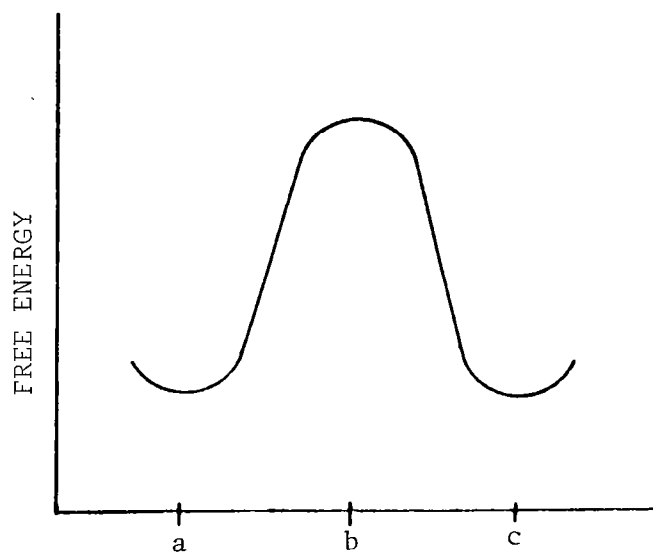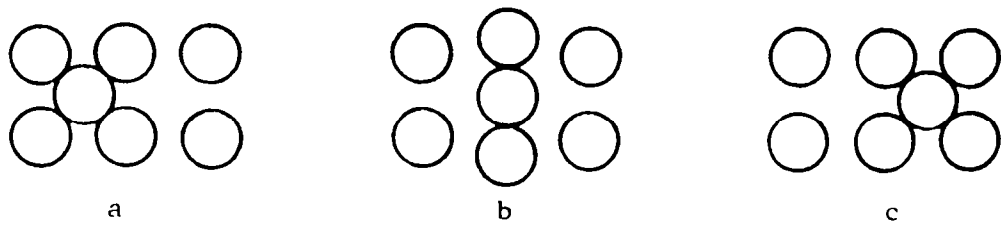
Free Energy Variation of Lattice During
Sequence of Atomic Motions Shown in a, b, and c

MECHANISM FOR AN ATOMIC JUMP INTO A VACANCY

Figure 2

The average jump frequency per atom, ω, becomes

$$\omega = N_m \bar{v} / \delta \qquad (23)$$

To find an approximate value of N_m, it is assumed that diffusing atoms enter, remain at, and leave the activated complex slowly so that the remainder of the lattice has time to continually relax to an equilibrium state.[21] Using this assumption, the work done during the resulting reversible, isothermal process of moving an impurity atom from one site to another is just equal to the change in the Gibbs free energy for the region, G_m. From these assumptions, at any temperature, there will always be an equilibrium number of activated complexes. From the definition of G_m, in equation (13)

$$G_m = H_m - TS_m \qquad (24)$$

Since the lattice was assumed to be in thermal equilibrium, G_m will have all of the properties of G_v of equation (17). By a process identical to the derivation of equation (19) from equation (17),[22] we can obtain the equilibrium mole fraction of activated complexes at any instant:

$$N_m = \exp \left| \frac{-H_m + T\Delta S_m}{RT} \right| = \exp \left| \frac{-\Delta G_m}{RT} \right| \qquad (25)$$

In equation (23), a dimensional analysis will reveal that $\bar{v}/\delta$ is a frequency. This frequency is conveniently taken to be the mean vibrational frequency of an atom about its

equilibrium site, ν, and represents the frequency with which
an atom attempts to change sites. From this and from
equations (23) and (25) we find

$$\omega = \nu \ \exp \ \frac{-H_m + T\Delta S_m}{RT} \qquad (26)$$

It has been determined experimentally that the
activated complexes do not exist long enough for much of the
surrounding lattice to reach equilibrium.[23] Thus, it would
seem that the basis for the derivation of equation (26) is
open to serious question. However, it does yield an order
of magnitude agreement with experiment.

C-2   Relationship Between Self-Diffusion and Dilute
        Impurity Diffusion

The problems involved with impurity diffusion are
more complex than those of self-diffusion, since the atoms
of both solvent and solute migrate simultaneously. The mi-
gration of solute atoms is influenced by that of solvent atoms,
and the presence of impurity atoms in the lattice, changes
the energy conditions, and thus influences the rate of self-
diffusion.

C-2.1   Correlation Effects: In dilute alloys, the
vacancies are partially bound to the solute atoms, so that
there is in addition to the correlation between the jumps of
the solute atoms a correlation between the successive jumps
of the vacancies. Thus, it is no longer possible for P_v to

equal N_v, although these two quantities are still closely
related. Also, the correlation coefficient becomes much
less than unity. In this discussion of impurity diffusion,
it is assumed that the solute concentration is so small
that the diffusion coefficient of the solute in the solvent
lattice, or the impurity diffusion coefficient, is inde-
pendent of the solute concentration. In analyzing the
behavior of a solute atom-vacancy pair in a solvent lattice
under these conditions, the frequency with which the solute
atom and vacancy exchange positions may be taken as ω_1, the
frequency with which the vacancy exchanges places with a
nearest neighbor atom to the solute atom as ω_2, and the
frequency with which the vacancy exchange places with a
solvent atom which is not a nearest neighbor to the solute
atom as ω_3. Thus ω_3 is proportional to the frequency at
which the solute atom-vacancy pair dissociates. Now if the
vacancy is tightly bound to the solute atom, ω_3 will be
nearly zero, and ω_1 will be much greater than ω_2. In other
words, if a vacancy exchanges places with a solute atom
with a given jump, the probability that it will reverse
that exchange with its next jump is nearly unity. If this
is so, the vacancy movement is nearly completely correlated,
and the solute atom will move through the lattice only as
fast as the vacancy exchanges with the solvent atoms. Thus,
the impurity diffusion coefficient for small solute con-
centrations, $D_I(0)$, will not be given by

$$D_I(0) \sim a_o^2 \omega_1 N_v$$

but by

$$D_I(0) \sim a_o^2 \omega_2 P_v = 2fa_o^2 \omega_1 P_v << a_o^2 \omega_1 P_v \quad . \tag{27}$$

The relationship between P_v and N_v is discussed on page 35. In the above equations $f << 1$, and the correlation effect becomes quite important. Note, the relation between the correlation coefficient, f, and the quantities ω_1, ω_2, and ω_3 is a function of the lattice geometry. As an example, we can consider a face centered cubic lattice, where the expression for f is given by[24]

$$f = \left| \frac{\omega_2 + 7\omega_3/2}{\omega_1 + \omega_2 + 7\omega_3/2} \right| \tag{28}$$

Here the return of the dissociated vacancy is ignored. The expression for $D_I(0)$ thus becomes

$$D_I(0) = \left| \frac{a_o^2 \omega_1 (\omega_2 + 7\omega_3/2)}{\omega_1 + \omega_2 + 7\omega_3/2} \right| P_v \quad . \tag{29}$$

Present day calculations of ω_2 and ω_3 yield ambiguous results, so the best practical approach is to estimate the value of $D_I(0)$ for several limiting cases.[25] These are:

(1) the rate of dissociation of solute atom vacancy pairs is much less than the exchange rate between the vacancy and the nearest neighbor to the solute atom, or $\omega_2 > \omega_3$. Then we have from from equation (29)

$$D_I(0) \sim a_o^2 \left| \frac{\omega_2 \omega_1 P_v}{\omega_1 + \omega_2} \right| \tag{30}$$

(2) the vacancy-solute atom exchange rate is much more
    rapid than the two vacancy-solvent atom exchange rates,
    or the vacancy-solute atom pair is tightly bound. Then
    $\omega_1 >> (\omega_2 + 7\omega_3/2)$ in (28), and we have

$$D_I(0) \sim a_o^2 (\omega_2 + 7\omega_3/2) P_v \qquad (31)$$

(3) the solute atom jumps slowly, or $\omega_1 << (\omega_2 + 7\omega_3/2)$ in
    equation (29). Thus

$$D_I(0) \sim a_o^2 \omega_1 P_v \qquad (32)$$

(4) the "solute" is a solvent tracer, so that $\omega_1 = \omega_2 = \omega_3 =$
    ω. Then, since here $P_v = N_v$, and $D_s(0) = D_I(0)$

$$D_s(0) = 2fa_o^2 N_v \omega \quad . \qquad (33)$$

It must be emphasized that the above results are
for a face centered cubic lattice. Other lattice geometries
will give results of essentially the same form, but with
different numerical constants.

C-2.2   <u>Valence Effects</u>: Due to the electronic effect of
an impurity atom with a valence different than that of the
surrounding host lattice a vacancy is often attracted to
the solute atom. Consider the case of a divalent impurity
in a monovalent lattice. According to the free electron
theory of metals the free electron density in the immediate
environment of the impurity will be greater than that
throughout the lattice as a whole, but it will not be great

enough to completely neutralize the excess positive charge of the solute ion. This ion is said to be "screened," and it is surrounded by an electrostatic potential of the form

$$V(r) = (Ze/r) \exp(-qV) \quad . \tag{34}$$

Where r is the radial distance from the impurity ion, Z is the number of excess electrons per impurity ion and q is the screening parameter, which gives a measure of the neutralization of the excess charge of the impurity ion. Let a solvent atom be removed from a site adjacent to the solute ion, and make the assumption that the electron distribution throughout the lattice will not be appreciably distributed by this removal. If this is the case, the vacancy resulting from this removal will have an effective charge of -e. Its energy on the site next to the impurity ion then will be reduced by

$$eV(r) = E(r) = (Ze^2/r) \exp(-qr) \tag{35}$$

as compared to a site surrounded by normal solvent atoms. Since the energy of the vacancy is lower next to the impurity ion, the concentration of vacancies on any nearest neighbor site will be increased to

$$P_v = N_v \exp(E(r)/kT) \quad . \tag{36}$$

This effect will also decrease H_v on a site next to a solute atom by E(r) as compared to H_v on a site surrounded by solvent atoms. This decrease in potential energy also makes

H_v for the solute less than H_v for the solvent. Finally, there is a force $e(dV/dr)$ tending to draw the vacancy and the impurity ion together. If the impurity ion and the vacancy begin to move together, this force tends to pull them together until H_v is decreased by roughly $r_o e(dV/dr)_{r=r_o}$.[26]

C-2.3   <u>Size Effects</u>: The effects on the impurity diffusion coefficient of the size of the solute atom relative to that of the solvent atom have been considered by Swalin[27] and Overhauser.[28]

Swalin assumes that the solute atoms are compressible spheres and the solvent lattice is an elastic continuum. For example, if the solute is larger than the solvent atom, H_v will be increased by the additional strain required at the saddle point. This change in H_v is a balance between the strain on the diffusing solute atom and the lattice continuum. Although it would seem that a large solute atom would elastically strain the lattice and thereby attract vacancies and lower H_v, Swalin concluded that the actual change in H_v is negligible to a first order approximation.[27]

Overhauser[28] considered the effects on the impurity diffusion coefficient of the presence of interstitials in the solvent lattice. Since these interstitials dilate the lattice locally, the average interatomic distance between the matrix atoms will be increased. This lattice expansion will reduce the work required to squeeze

an atom through the saddle point, so H_v should be decreased by the addition of an interstitial solute whose atoms are larger than those of the solvent. Likewise, the addition of an interstitial solute which contracts the solvent lattice should increase H_v.

Although the impurity diffusion concept has been studied in detail for many elements, no single correlation between diffusion parameters D_o, the frequency factor, and Q, the activation energy and the properties such as valence and size has been found to fit more than one or two elements.

C-2.4   Solute Concentration Effects: When the solute concentration becomes greater than some threshold value, (which varies for different systems), the solute atoms begin to interact and the diffusion coefficient for the solute as well as the self-diffusion coefficient for the solvent material becomes a function of the solute concentration. In order to obtain a qualitative concept of the nature of these functions, we consider the previously presented equations for the self-diffusion of the pure solvent, (33), and the dilute impurity diffusion coefficient for the solute, in a face centered cubic solvent lattice, (28), i.e.,

$$D_S(0) = 2fa_o^2 \omega_o N_v \tag{33}$$

and

$$D_I(0) = 2 \left| \frac{a_o^2}{1} \frac{(\omega_2 + 7\omega_3/2)}{\omega_1 + \omega_2 + 7\omega_3/2} \right| P_v \quad . \tag{28}$$

Now if $P_v = N_v$ and $\omega_1 \sim \omega_2 - \omega_3$, then no matter how large ω_1 is, $D_s(0)$ will about equal $D_I(0)$. However, if $D_I(0)$ is greater that $D_s(0)$ in very dilute alloys, it follows that the impurity atoms attract vacancies so that $P_v > N_v$. Then the solvent jump frequencies ω_2 and ω_1 are increased near a solute atom. But if $P_v > N_v$, or $\omega_2 > \omega_0$ near a solute atom, then D_s is also greater near a solute atom. As the solute concentration increases, so does the number of affected solvent atoms. Thus, if $D_I(0) < D_s(0)$, an addition of solute will increase D_s. Similarly, if $D_I(0) > D_s(0)$, an addition of solute will decrease D_s.

To provide an estimate of the magnitude of the change in the self-diffusion coefficient, D_s, with solute concentration, the following empirical equations have been derived for solute concentration ≤ 0.01:[29]

$$D_s = (1 - AN_I)(D_s(0)) + A\beta N_I D_I \qquad (37)$$

$$D_I = D_I(0) \qquad (38)$$

Here, N_I is the solute concentration, A is the number of nearest neighbor sites around each atom, and β is an arbitrary constant ≤ 1.0 which must be experimentally determined. Thus, D_I does not vary much with solute concentration for solute concentrations less than 0.01. For solute concentrations greater than 0.01, the relation between the impurity diffusion coefficient and solute concentration is given by

$$D_I = D_I(0)(1 + \mu N_I) \qquad (39)$$

Here, μ is a constant ≤ 1.0. The values of the constants β and μ vary from system to system. Specific theoretical calculations of their values are quite difficult and are not usually attempted.

D. Summary of Equations for Diffusion Coefficient

The following comprise a summary of the most useful previously derived diffusion relationships which are most useful in comparing experimentally observable parameters with theoretical models for the diffusion process.

For vacancy self-diffusion in a pure solvent with correlated tracer jumps, the self-diffusion coefficient, D_s, is given by

$$D_s(0) = 2fa_o^2 N_V \omega \tag{40}$$

where f is the correlation coefficient, N_V is the equilibrium vacancy concentration, ω is the tracer jump frequency, and a_o is the lattice constant. For dilute impurity vacancy diffusion, the diffusion coefficient of the solute in the solvent lattice is

$$D_I(0) = 2fa_o^2 \omega_1 P_V \tag{41}$$

Here ω_1 is the frequency with which a solute atom changes places with a nearest neighbor vacancy, and P_V is the probability that a nearest neighbor site to the impurity atom is vacant. Because of attractive forces between the vacancies and solute atoms have already been discussed, P_V

in equation (27) will not equal N_v. An estimate of the
value of P_v in terms of N_v for a given solvent-solute sys-
tem may be obtained from equations (33), (34), and (35).
The coefficient of correlation f is a function of lattice
geometry. For self-diffusion, f lies between 0.50 and 0.79;[15]
for a face-centered cubic solvent structure, f for impurity
vacancy diffusion is given by

$$f = \frac{\omega_2 + 7\omega_3/2}{\omega_1 + \omega_2 + 7\omega_3} \qquad (42)$$

Here ω_2 is the frequency with which a vacancy exchanges
position with a nearest neighbor atom to a solute atom, and
ω_3 is the frequency with which a vacancy exchanges position
with a solvent atom, which is not a nearest neighbor to a
solute atom.

From equilibrium thermodynamics, the equilibrium
vacancy concentration in a crystal was found to be

$$N_v = \exp \frac{\Delta S_t}{R} \exp \frac{-H_v}{RT} \qquad . \qquad (43)$$

In a similar manner, an equilibrium approximation allowed
us to arrive at an expression for

$$\omega = \nu \exp \frac{-H_m + T\Delta S_m}{RT} \qquad . \qquad (44)$$

Combining equations (19), (26), and (40) allows us to write
for the vacancy self-diffusion coefficient in a pure or
very dilutely contaminated solvent

$$D_s(0) = 2fa_o^2 \nu \exp \left| \frac{\Delta S_f + \Delta S_m}{R} \right| \exp \left| \frac{-H_f - H_m}{RT} \right|. \qquad (45)$$

Likewise, combining equations (19), (26), (27), and (35), we find for dilute impurity vacancy diffusion

$$D_I(0) = 2fa_o^2 \nu \exp \left| \frac{\Delta S_f + \Delta S_m}{R} \right| \exp \left| \frac{-H_f - H_m}{RT} \right| \exp \left| \frac{E(r)}{kT} \right|.$$
$$(46)$$

Here $E(r)$ may be estimated from equation (34), and f for a fcc lattice is given by equation (28). Generally, f will be given in terms of the various jump frequencies described above. Of these frequencies, only ω_1 can be calculated with reasonable certainty; because of uncertainties in the values of ω_2 and ω_3, the usual practice is to consider the behavior of $D_1(0)$ in the limiting cases given in equations (30), (31), and (32).

Equations (37), (38), and (39) give the variation in the solvent self-diffusion coefficient $D_s(0)$, and vacancy impurity diffusion coefficient, $D_I(0)$, with solute concentration. Finally, for interstitial diffusion, the diffusion coefficient, D, is given by

$$D = a_o^2 \nu \exp \left| \frac{\Delta S_m}{R} \right| \exp \left| \frac{-H_m}{RT} \right| \qquad . \qquad (47)$$

Thus, interstitial diffusion can be considered a much simpler process than vacancy diffusion. For the present investigation it is probable that both vacancy and interstitial diffusion mechanisms take place.

Equations (45), (46), and (47) are useful in cal-
culating values of D from theoretical models of the diffusion
process. To check the validity of a given model, a compari-
son is made of the calculated values of the factors compri-
sing D with corresponding experimentally determined values.
Several workers have devised experimental methods for deter-
mining the individual terms of equations (45), (46), and
(47), such as ΔS_f, ΔS_m, H_m, etc.. However, the most common
procedure is first to express these equations in the form

$$D = D_o \exp (-Q/RT) \quad . \quad\quad (48)$$

Then, after determining the diffusion coefficients of the
system under consideration at different temperatures, Q may
be found from the slope of the plot of the natural logarithm
of D versus (temperature, ^oK)$^{-1}$, while the intercept of this
plot with the ordinate axis yields D_o. The quantity Q is
called the activation energy, and is the sum of the enthalpy
terms in each of the equations for D, (45), (46), and (47).
This quantity is thus associated with the energy necessary
for the solute ion to make a single jump in the solvent lat-
tice. The symbol, D_o, called the frequency factor, contains
the correlation coefficient, jump attempt frequency, lattice
parameter, and the entropy changes associated with an atomic
jump. Hence, D_o gives a measure of the disorder induced in
the solvent lattice by an atomic jump.

The " random walk " is not the only approach for the explanation of the phenomena of diffusion. Some of the more interesting theories are presented by: Feit discusses a dynamical theory,[30,31] Huntington and Seitz with a discussion from the modern theory of metals,[32] Lazarus discusses the effect of " screened " electrons on diffusion,[33] Johnson presents a " hole " theory for diffusion,[34] while Zener presents a model for ring diffusion.[35] All of these studies present arguments which are valid for some very limited cases and were therefore not used in this work. For further reading on diffusion, the studies by LeClaire[36], Wert and Zener,[37] Turnbull and Hoffman,[38] and Zener[39] are suggested.

Part III

MATERIALS AND APPARATUS

This research depended upon mass spectrometric instrumentation of high sensitivity. It was also conditioned by the type and form of samples which were amenable to diffusion analysis by mass spectrometric means.

The samples of zircaloy-2, tantalum, and 304 stainless steel ribbon were obtained from H. Cross Company of Weehawken, New Jersey, with a detailed analysis of the composition of each sample material. These appear in Tables I, II, and III.

The mass spectrometer used in this research was a 90° double focusing instrument with a resolution of approximately 1/1000, designed and built by F. A. White and J. C. Sheffield.[40]

A. Description of the Filament

A single filament thermal ionization source, Figure 3, was used in all experiments. Each of the three sample materials (304 stainless steel, zircaloy-2, and tantalum) were used as the filament material. The ribbons of the zircaloy-2 and tantalum were 0.030" (0.076 cm) x 0.001" (0.0025 cm), while the 304 stainless steel ribbon was 0.030" (0.076 cm) x 0.0005" (0.0013 cm).

Heremetically sealed, insulated feedthrus, on which the filament ribbons were spot-welded, were obtained from Electrical Industries, Murray Hill, New Jersey. The

Table I

COMPOSITION OF 304 STAINLESS STEEL

Carbon	.056%
Manganese	1.65 %
Phosphourus	.018%
Sulphur	.012%
Silicon	.49 %
Chromium	18.53 %
Molybdenum	.31 %
Copper	.25 %
Nickel	9.14 %
Cobalt	.03 %

Table II

COMPOSITION OF TANTALUM

TANTALUM

Ta

Atomic Number	73
Atomic Weight	180.95
Crystal Structure	BCC
Melting Point °C	2996
Density gms/cc (20°C)	16.6
lbs./in^3	0.600

MARZ GRADE

MATERIALS ANALYSIS

Analysis: ■ Mass Spectrographic ■ Vacuum Fusion (Gases) □ Emission Spectrographic ■ Conductometric (Carbon)

Element	Content (ppm)	Element	Content (ppm)	Element	Content (ppm)	Element	Content (ppm)
O	< 5.0	S	2.0	Cu	0.3	Sn	0.2
C	< 5.0	Cl	2.0	Zn	< 0.1	Te	< 0.2
H	< 5.0	K	0.1	Ge	< 0.4	I	< 1.0
N	< 3.0	Ca	0.4	As	< 0.1	W	3.0
B	< 0.1	Sc	< 0.1	Br	< 1.0	Pt	< 5.0
F	< 1.0	Ti	< 1.0	Zr	< 1.0	Au	< 5.0
Na	< 0.4	V	0.2	Nb	20.0	Pb	< 0.6
Mg	< 0.2	Cr	3.0	Mo	< 0.5	Bi	< 0.3
Al	0.5	Mn	< 1.0	Ag	< 0.4	Co	< 0.3
Si	0.7	Fe	10.0	Cd	< 0.3	All	
P	0.3	Ni	1.0	In	< 0.2	others	< 0.1

METHOD OF PREPARATION: Electron Beam
Zone Refined

NOMINAL PURITY (TOTAL): 99.996%

STANDARD SINGLE CRYSTALS

	$/in. (1" Minimum Order)			
diameter	⅛"	¼"	⅜"	½" (.450")
	$100.	$125.	$150.	$225.

Random Orientation. Oriented crystals, $75. additional orientation charge per crystal, independent of length. (100), (110), and (111) available.

SPECIAL APPLICATION CRYSTALS

Cut from ½" nominal diameter (elliptical cross-section) to approximately ⅛" thickness, one face polished strain-free to expose specified crystallographic plane:

Within 1° $650./slice; additional slices of same orientation $200. each.
Within 4° $325./slice; additional slices of same orientation $150. each.

POLYCRYSTALLINE RODS

diameter	in./lb.	gms/in.	< 100 gms $/gm	100-300 gms $/gm	1-3 lbs. $/lb.	> 3 lbs.
⅛"	137	3.32	$3.00	$1.70	$550.	$500.
¼"	34	13.27	2.00	1.60	500.	450.
⅜"	15	29.84	1.85	1.55	475.	425.
½"	8.5	53	1.75	1.45	450.	400.
1"	2.1	2.20	—	1.38	400.	350.

> lb. on request.
Minimum Order: $50.00

TABLE III

COMPOSITION OF ZIRCALOY-2

ZIRCALOY-2 INGOT
HEAT NO. 387266

COMPOSITION IN PERCENT		
	Top	Bottom
Sn	1.45	1.48
Fe	0.15	0.16
Cr	0.11	0.11
Ni	0.05	0.06
Zr	B A L A N C E	
IMPURITIES IN PPM		
Al	47	49
B	0.2	0.2
C	110	100
Cd	<0.2	<0.2
Co	<10	<10
Cu	16	15
H	7	<5
Hf	41	39
O	1180	1150
Mn	<25	<25
N	46	38
Si	73	79
Ti	<25	<25
W	<25	<25
U	1.5	1.8
V	<25	<25

INGOT HARDNESS, BHN	
Range	170 - 179
Average	176
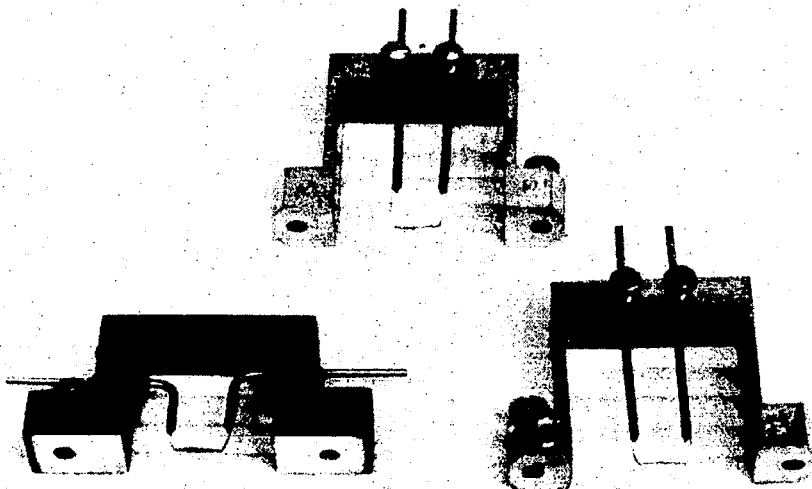
SINGLE FILAMENT THERMAL IONIZATION SOURCE

FIGURE 3

feedthrus are designated as EI type A-40W-SS Mod H.

B. The Mass Spectrometer

The mass spectrometer separates chemical elements according to their mass to charge ratio. The mass spectrometer shown in Figure 4 was used exclusively in this study. A schematic of this two-stage, double focusing instrument is shown in Figure 5. The major components of the instrument include:

    (a) Ion source
    (b) Electrostatic analyzer
    (c) Magnetic analyzer
    (d) Beam defining slit system
    (e) Ion detector and counting system
    (f) Vacuum system

Thermal Ionization. For mass spectrometric analysis, some method is needed to vaporize and ionize the sample into a beam of positively charged ions before entering the electrostatic and magnetic filters. For the analysis of metals, thermal ionization is an effective means of producing gaseous ions especially if the metal has a low ionization potential compared to the filament's work function. As the sample vaporizes, some atoms or molecules will leave the surface of the filament with the loss of one or more of their electrons. The hot filament surface has a higher affinity for electrons than the metal itself. This is due in part, to the intrinsic nature of the metallic crystal along with the low binding energy of the outer shell electrons of most metallic atoms.
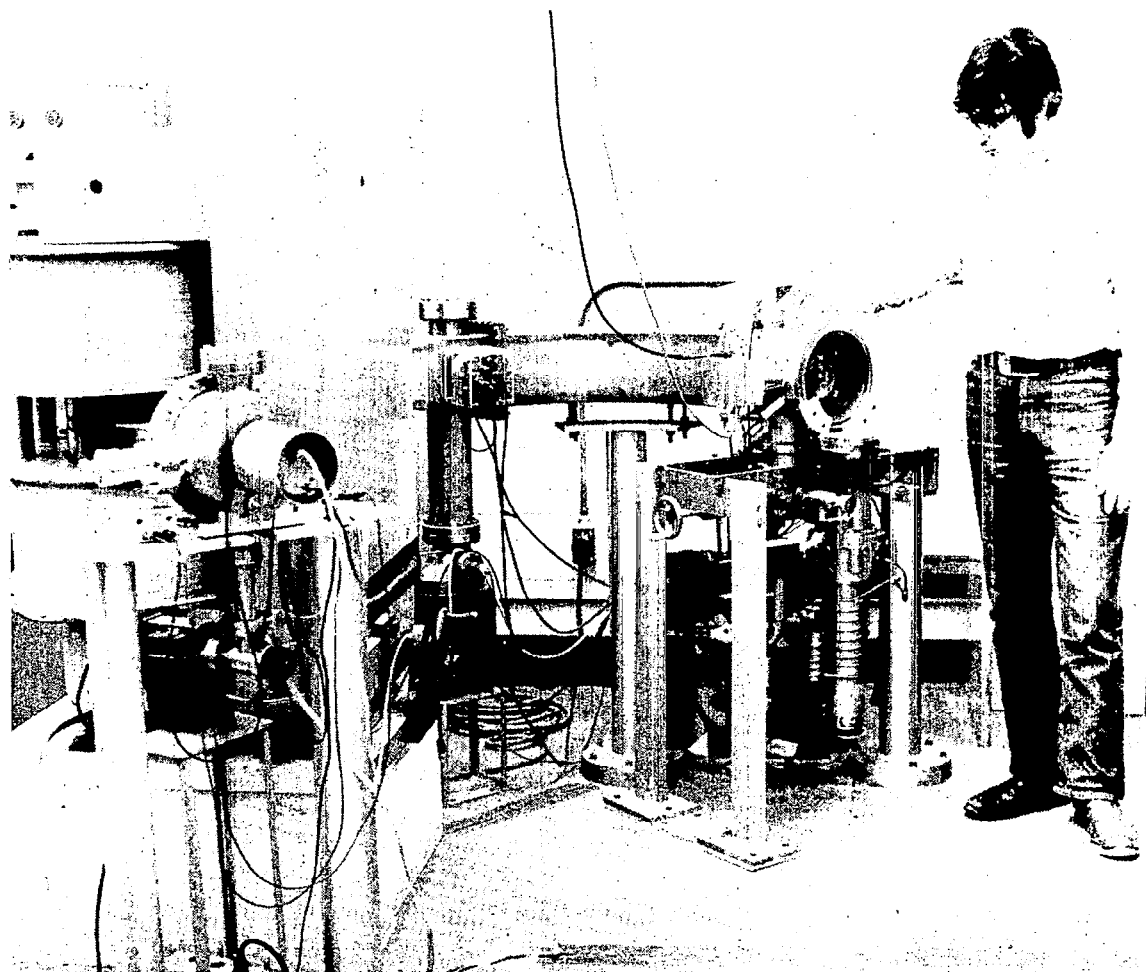
TWO-STAGE MASS SPECTROMETER

FIGURE 4

AMPLIFIER / DISCRIMINATOR / DRIVER

DATA ACQUISITION SYSTEM

FINAL SLIT SYSTEM

ELECTRON MULTIPLIER & BRIDGE CIRCUIT

15 L/S VACION PUMP

MAGNETIC ANALYZER
50.8 CM. RADIUS OF CURVATURE

ION SOURCE

GATE VALVE

CENTER SLIT SYSTEM

10.16 cm DIFFUSION PUMP

75 L/S VAC ION PUMP

ELECTROSTATIC ANALYZER
50.8 CM. RADIUS OF CURVATURE
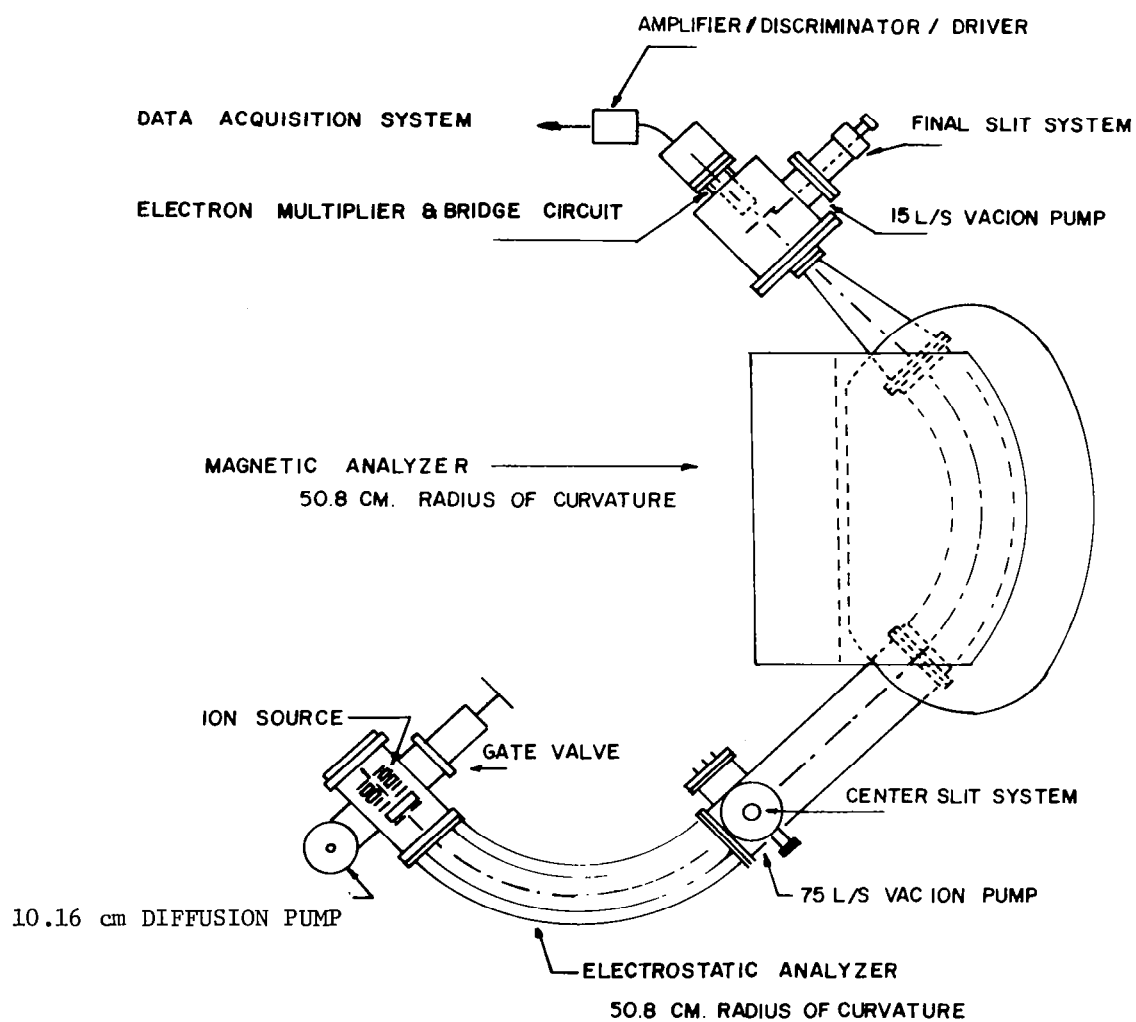
Two Stage, Double Focusing Mass Spectrometer

Figure 5

44

The probability of an atom evaporating from a sur-
face in the ionic state rather than as a neutral atom is
expressed by the relation,

$$\frac{n^+}{n^o} \propto \exp \frac{e(\phi - IP)}{kT} \propto \exp \frac{11606 \ (\phi - IP)}{T} \qquad (49)$$

where n^+ is the number of positive ions, n^o is the number of
neutral specie, e is the electron charge, IP is the ioniza-
tion potential of the sample in electron volts, ϕ is the
surface work function of the filament material in electron
volts, k is Boltzmann's constant, and T is the surface
temperature in ^oK.

It can be seen that for elements where $IP > \phi$ the
relative number of ions to neutrals produced will increase
with temperature.

Ions resulting from thermal ionization on the
filament surface are accelerated to high energy and defined
by collimating slits in the ion source. These high energy
ions pass through the electrostatic analyzer where they are
energy filtered. Ions with a discrete kinetic energy
(accelerating voltage) including a small energy spread
pass through the center defining aperture. The defining
slit determines the energy spread accepted. This filtered
beam of ions then enters the magnetic analyzer where the
beam is momentum filtered. Those ions of appropriate
energy and proper momentum (essentially mass) come to a
focus at the final slit and strike an electron multiplier.

Current pulses result from ion-electron conversion and sub-
sequent secondary electron amplification in the electron
multiplier tube. Output pulses are further amplified and
counted by an amplifier/discriminator/scalar system. Thus,
ions of the same mass are individually counted and the
exceedingly small ion currents can be quantitatively
measured.

By properly changing the accelerating potential
of the ion source, ions of other mass numbers are focused
on the electron multiplier. By comparing counting rates
for each mass position the isotopic ratio can be quantita-
tively determined.

Part IV

EXPERIMENTAL METHOD

A. General Experimental Techniques

From the literature, the most common method for ob-
taining diffusion coefficients is that of serial sectioning.
However, a mass spectrometric approach was chosen for this
work. The basic concept of the mass spectrometric technique
for determining diffusion coefficients is that a correlation
exists between the solute atoms moving through a solvent
lattice and the fraction of these atoms which are evaporated,
as ions, from the crystal surface at a given temperature.

In this work, a thin ribbon filament of solvent
material is used with its own impurity or solute concentra-
tion. No doping of the solvent was required and thus there
was no alteration of the crystal lattice. Since the mass
spectrometer source chamber pressure is well below the vapor
pressure of the solute material in the temperature range con-
sidered, the solute atoms diffuse to the filament surface,
and evaporate immediately. This results in a zero solute
concentration at the filament surface after the filament
temperature is raised to the desired level. Further, as the
ribbon thickness is much less than its length or width, the
diffusion problem may be considered to be one dimensional.

Application of Fick's Second Law for Diffusion

in a Thin Plate: Since the solute concentrations

47

under consideration are very small, the diffusion process occurring in the ribbon may be described by

$$J(x,t) = -D \frac{\partial C(x,t)}{\partial x} \qquad (50)$$

and

$$\frac{\partial C(x,t)}{\partial t} = -D \frac{\partial^2 C(x,t)}{\partial x^2} \qquad (51)$$

where $J(x,t)$ is the solute flux, $C(x,t)$ is the solute concentration, and D is the diffusion coefficient. For the experimental conditions previously described, the solution to Fick's second law for impurity evaporation from a thin plate yields the solute concentration, as a function of position in the filament and evaporation time, t.

Solving equation (51) by the method of separation of variables, the solute concentration may be found to be

$$C(x,t) = (A \sin \lambda x + B \cos \lambda x) \exp (-\lambda^2 Dt) \qquad (52)$$

where $\lambda^2 = -(1/dT)(dT/dt)$ or $-(1/X)(d^2X/dx^2)$, D is the diffusion coefficient, t is time, and A and B are constants of integration.

For solute depletion from a thin solvent plate with an initial solute concentration $f(x)$ across its thickness, the boundary and initial conditions become

$$C = 0 \text{ at } t \geq 0, \text{ for } x = h \text{ and } x = 0$$
$$C = f(x) \text{ at } t = 0, \text{ for } h > x > 0$$

With these conditions, equation (52) becomes

$$C(x,t) = \frac{2}{h} \Sigma \sin \frac{n\pi x}{h} \exp \left| \frac{-D\pi^2 n^2 t}{h^2} \right| \int f(x') \sin \frac{n\pi x'}{h} dx'$$

$$(53)$$

Where h is the filament thickness. Thus from Fick's first law, equation (50), the solute atom flux at the filament surface (x=0) becomes

$$J(0,t) = (2/h) \Sigma \exp \left| \frac{-D\pi^2 n^2 t}{h^2} \right| \int f(x') \sin \frac{n\pi x}{h} dx' \qquad (54)$$

or more conveniently, where n is an integer,

$$J(0,t) = A \Sigma \exp \left| \frac{-D\pi^2 n^2 t}{h^2} \right| \qquad (55)$$

where A is a constant. For $h^2 < 16Dt$ the error in using only the first term is less than 1%.[41]

Positive Ion Emission from a Hot Metal Filament:
The combination of high temperature and solvent work function causes a constant fraction of the evaporating solute atoms to ionize at the filament surface at a given temperature. According to the Langmuir-Saha equation, the ratio of the number of emitted positive ions (n^+) to emitted neutrals (n^o) is

$$n^+/n^o = B \exp \{(\phi - IP)/kT\} \qquad (56)$$

where B is a proportionality constant, ϕ is the filament work function, IP is the ionization potential for the solute, k is Boltzmann's constant, and T is the temperature of the filament in degrees Kelvin.[42]

The mass spectrometer accelerates, mass analyzes, and detects these emitted solute ions while excluding all other ionic species from its detector. By combining equations (54) and (55), and assuming that the atomic transport time is greater than $h^2/16Dt$, the time variation of the

detected ion current is

$$J(0,t) = A \exp (-\pi^2 Dt/h^2) . \qquad (57)$$

B. Experimental Procedures

The procedures used in this work are detailed
below to allow reproduction of the experiments. A general
procedure followed at all times was the wearing of lintless
gloves when handling anything going into the vacuum environ-
ment. The procedures described are:

      1. Cleaning
      2. Spotwelding
      3. Mass spectrometry
      4. Calibration of mass spectrometer
      5. Filament temperature measurement
      6. Data acquisition
      7. Treatment of data
      8. Error analysis

1. Cleaning:

Filament holders: Clean metal surfaces with 4M HNO_3,
and rinse with de-ionized water.
Dry under the infrared lamp.

Filament legs : Place in an alcohol bath immersed
in the ultrasonic cleaner. Rinse
with de-ionized water and dry under
an infrared lamp.

2. Spotwelding:

By visual inspection, make sure electrodes are clean

Set to 18-25 watt-seconds

Place one end of filament next to the supporting legs
and then spotweld

Do the same for the other end of the filament and leg

3. **Mass Spectrometer**:

Opening Source Region:

      Close main gate valve, isolation valve, and the roughing valve

      Open the foreline valve

      Connect up nitrogen gas, turn on, and let it into the source chamber

      Let chamber come to atmosphere, put clips on O-ring

      Before dismantiling anything, make sure power is OFF

      Screw filament assembly onto the top plate of the ion source.

Closing Source Section and Vacuum Pump Down:

      Make sure no lint is on O-ring or glass, and then put glass back on

      Turn nitrogen gas off and close inlet valve

      Open roughing valve, let it run for a few minutes

      Close roughing and open foreline valve

      Turn on first ionization gauge

      Make sure liquid nitrogen is in cold trap

      Open up the diffusion pump valve, do this SLOWLY and watch pressure gauge

      Turn on automatic ionization gauge

Opening System and Operation:

      Open isolation valve to system, after chamber pressure has reached 5×10^{-7} torr

      Set electron multiplier tube to -4500 volts

      Close gate valve on multiplier tube's ion pump

      Turn on polarity switch to minus, on the electro-static lens power supply

      Turn on main power to mass bridge (ion source voltage divider)

Turn voltage control on filament heater, adjust
current control for the temperature setting

Turn up voltage to desired setting, CAREFULLY

Begin data acquisition

System Shut Down:

Turn all voltage settings OFF

Close isolation valve

Open ion pump to electron multiplier tube

Turn multiplier tube voltage to -500 volts

Close diffusion pump gate valve

Turn OFF all power

Note: Liquid nitrogen will evaporate away

4. Calibration of the Mass Spectrometer:

It is necessary to calibrate the mass spectrometer
before undertaking any experiments measuring diffusion coef-
ficients. Using equation

$$B^2R^2 = (144)^2(mV_a) \tag{58}$$

where B is the magnetic field in gauss, R is the radius of
curvature (in cm.) of the magnetic analyzer, m is the mass
of the isotope of interest in amu., and V_a is the accelerating
potential in volts, the appropriate magnetic field-accelerating
potential values for a given mass can be determined.

Since the alkali metal atoms were to be examined,
calibrations were made using filaments which had solutions of
either rubidium or cesium evaporated on them. Rubidium has
two naturally occurring isotopes, mass 85 and mass 87. De-
tection of one mass and calculation of the magnetic field
allowed the determination of the accelerating potential of

the other isotope with the same magnetic field. In practice, an accurate calibration requires many repetitive measurements. Cesium-133 is the only stable isotope of cesium, and provides an accurate determination of the magnetic field.

Ion implanted, as well as micro-pipetted filaments of Cs-133 were also used for calibration purposes. The identical method was followed.

5. Filament Temperature Measurement:

Using a precision optical pyrometer, filament temperatures were determined by visually matching the color of the filament with the color of a calibrated, resistively heated wire within the pyrometer. It is accurate to within $\pm 3^{\circ}C$.

6. Data Acquisition Procedure:

The mass spectrometer data was obtained as follows:

1. The sample filament was placed in the ion source and the source chamber pressure was evacuated to a pressure of about 10^{-7} torr.

2. The source voltage was set at the accelerating potential of the desired diffusing isotope.

3. The filament was raised in temperature until ions were detected at the given accelerating potential. The filament temperature was then determined.

4. The ion emission rate as a function of time was monitored until a slowly decreasing emission rate was observed. The latter indicated that the maximum emission rate had occurred and the exponential decay portion predicted by diffusion theory, had been reached.

5. At this point, the ion current was recorded for one second every four seconds utilizing a frequency-period-counter which has an accuracy of ± 1 count.

6. The procedure was repeated for successively higher temperatures.

7. Treatment of Data:

A graph of the natural logarithm of the impurity ion current (represented by counts per second) from a particular solvent lattice versus time, for each temperature was plotted

The slope of the " linear best fit" line through the data was calculated

The diffusion coefficient was then calculated by

$$(\text{ slope of the line }) \cdot (\text{ thickness of filament}/\pi)^2$$

$$= -D$$

A graph was made of the ln D versus $10^4/T(^{\circ}K)$

Utilizing a PDP 8/I computer, the linear best fit line to the data points was made. The y-intercept of this line is the frequency factor, D_0, and was calculated by the computer. The correlation co-efficient of the data to the line was also calculated.

The activation energy, Q, was determined by multi-plying the slope of the line from the line in the preceding step by the Rydberg gas constant in units of kcal/mole/$^{\circ}K$.

8. Error Analysis:

Programs were written to provide the linear best fit line from a set of data points. The program also gave the detree of fitness in the form of a correlation coefficient. All error values were determined by calculating the product-moment coefficient of correlation and using a 95% confidence level. A final program was written to obtain the standard deviation for the activation energies. These programs appear in Appendix 1 and 2.

Part V

RESULTS AND DISCUSSION

Following the procedure previously indicated, graphs of the ln (alkali metal ion count rate) versus time were obtained. Figure 6 is an example of how the ion count rate varies with time. These superposed curves illustrate the detection of singly charged, mass resolved ions at several temperatures. The counting rates are relative, but most experimental measurements were in the region of 10^{-14} to 10^{-17} amperes, corresponding to counting rates of 10^5 to 10^2 ions per second.

Tables IV, V, and VI show the experimental results for the diffusion of the alkali metals in 304 stainless steel, tantalum, and zircaloy-2. All five naturally occurring alkali metals were found in tantalum and in 304 stainless steel; however, lithium was not found in sufficient quantities to determine its diffusion parameters in the zircaloy-2 sample.

Activation energy plots for these diffusion systems are shown in Figures 7 thru 20. The frequency factor, D_o, and the activation energy, Q, were calculated from these plots and are presented in Tables VII, VIII, and IX.

The data derived from the activation energy plots can be applied to the metallurgy of the system. For example, a sharp discontinuity can be attributed to an allotropic phase change in the host material. Since pure zirconium has

10^4

10^3

10^2

10

COUNTS PER SECOND

2

3

4

1

Rb^{85} DIFFUSION THRU TYPE 304 STAINLESS STEEL

RUN NO.	TEMP °C
1	903
2	958
3	1052
4	1116

TIME (5 SECOND INTERVALS)
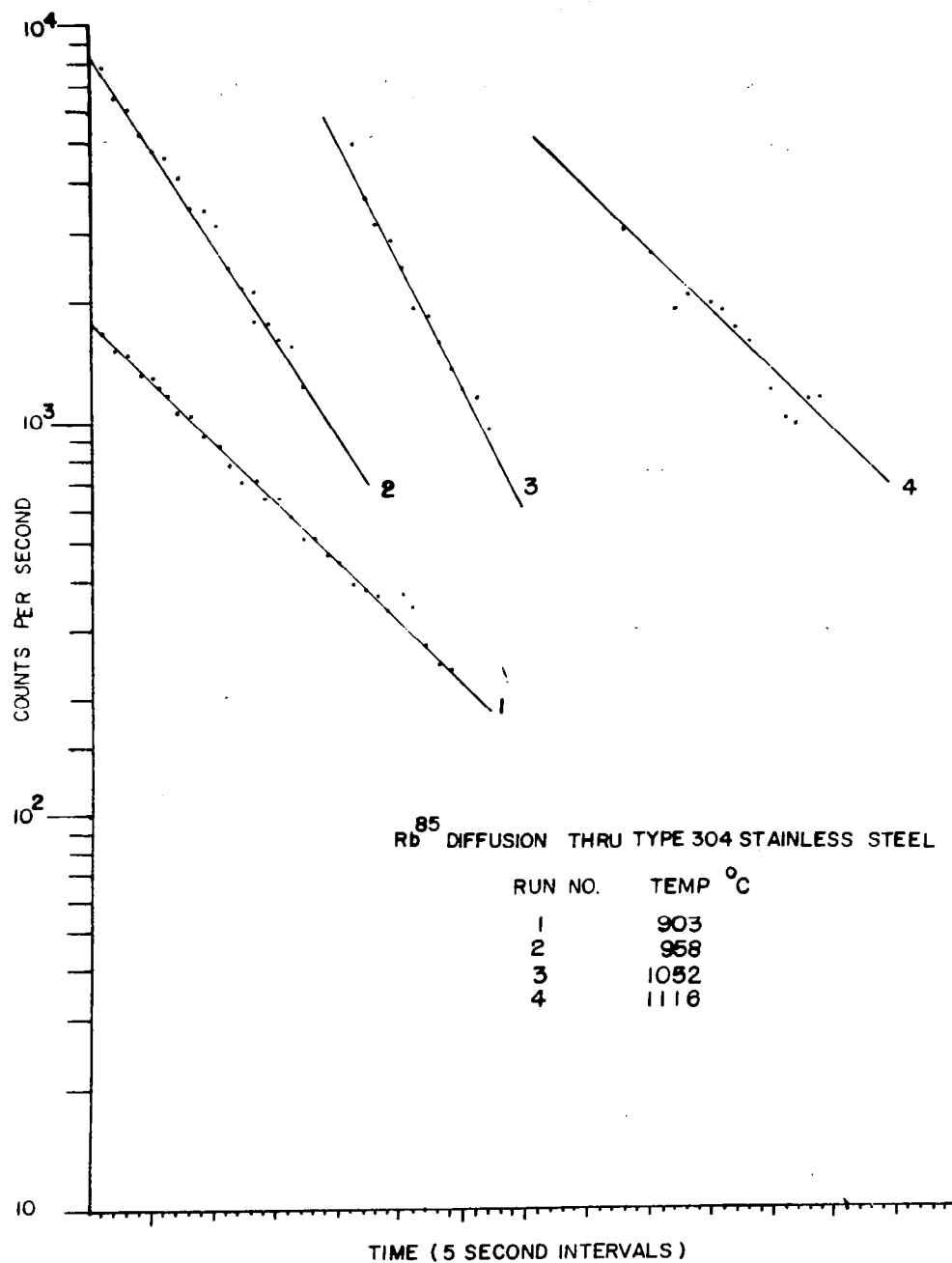
DIFFUSION OF Rb IN TYPE 304 STAINLESS STEEL

FIGURE 6

TABLE IV

DIFFUSION COEFFICIENTS OF THE ALKALI METALS IN TANTALUM

Li-7

$T(^oK)$	$D(cm^2/sec)$	$T(^oK)$	$D(cm^2/sec)$
1080	$4.52 \cdot 10^{-9}$	1522	$1.06 \cdot 10^{-8}$
1107	$5.03 \cdot 10^{-9}$	1534	$7.23 \cdot 10^{-9}$
1152	$6.86 \cdot 10^{-9}$	1570	$1.23 \cdot 10^{-8}$
1179	$1.10 \cdot 10^{-8}$	1575	$8.37 \cdot 10^{-9}$
1289	$1.91 \cdot 10^{-8}$	1605	$1.31 \cdot 10^{-8}$
		1621	$1.01 \cdot 10^{-8}$
1381	$3.08 \cdot 10^{-9}$	1650	$1.34 \cdot 10^{-8}$
1439	$4.37 \cdot 10^{-9}$	1650	$1.13 \cdot 10^{-8}$
1449	$4.77 \cdot 10^{-9}$	1669	$1.34 \cdot 10^{-8}$
1462	$7.70 \cdot 10^{-9}$	1675	$1.43 \cdot 10^{-8}$
1481	$7.18 \cdot 10^{-9}$	1721	$2.68 \cdot 10^{-8}$
1490	$5.58 \cdot 10^{-9}$	1802	$3.76 \cdot 10^{-8}$
1520	$8.92 \cdot 10^{-9}$		

K-39

$T(^oK)$	$D(cm^2/sec)$	$T(^oK)$	$D(cm^2/sec)$
1110	$1.24 \cdot 10^{-9}$	1471	$4.77 \cdot 10^{-9}$
1145	$2.18 \cdot 10^{-9}$	1495	$6.78 \cdot 10^{-9}$
1172	$3.47 \cdot 10^{-9}$	1497	$4.52 \cdot 10^{-9}$
1199	$4.18 \cdot 10^{-9}$	1499	$5.49 \cdot 10^{-9}$
1235	$4.64 \cdot 10^{-9}$	1524	$7.23 \cdot 10^{-9}$
1247	$7.44 \cdot 10^{-9}$	1529	$6.06 \cdot 10^{-9}$
		1577	$9.46 \cdot 10^{-9}$
1267	$2.02 \cdot 10^{-9}$	1595	$9.04 \cdot 10^{-9}$
1300	$2.04 \cdot 10^{-9}$	1616	$1.29 \cdot 10^{-8}$
1314	$2.51 \cdot 10^{-9}$	1664	$1.26 \cdot 10^{-8}$
1342	$2.55 \cdot 10^{-9}$	1672	$1.45 \cdot 10^{-8}$
1355	$3.78 \cdot 10^{-9}$	1718	$1.45 \cdot 10^{-8}$
1383	$2.86 \cdot 10^{-9}$	1745	$2.55 \cdot 10^{-8}$
1403	$4.01 \cdot 10^{-9}$	1767	$2.00 \cdot 10^{-8}$
1422	$4.11 \cdot 10^{-9}$	1828	$2.64 \cdot 10^{-8}$
1447	$4.36 \cdot 10^{-9}$		

Na-23

$T(^oK)$	$D(cm^2/sec)$	$T(^oK)$	$D(cm^2/sec)$
1033	$7.31 \cdot 10^{-9}$	1311	$3.27 \cdot 10^{-9}$
1058	$7.66 \cdot 10^{-9}$	1330	$3.30 \cdot 10^{-9}$
1107	$7.94 \cdot 10^{-9}$	1348	$4.69 \cdot 10^{-9}$
1110	$8.01 \cdot 10^{-9}$	1377	$4.46 \cdot 10^{-9}$
1140	$1.32 \cdot 10^{-8}$	1464	$4.71 \cdot 10^{-9}$
1176	$1.68 \cdot 10^{-8}$	1466	$6.39 \cdot 10^{-9}$
1190	$1.23 \cdot 10^{-8}$	1488	$5.97 \cdot 10^{-9}$
1230	$1.66 \cdot 10^{-8}$	1490	$2.99 \cdot 10^{-9}$
1230	$1.63 \cdot 10^{-8}$	1527	$6.86 \cdot 10^{-9}$
		1610	$1.23 \cdot 10^{-8}$
1238	$2.80 \cdot 10^{-9}$	1634	$1.31 \cdot 10^{-8}$
1289	$2.10 \cdot 10^{-9}$	1661	$1.09 \cdot 10^{-8}$
1290	$2.90 \cdot 10^{-9}$		

Rb-85

$T(^oK)$	$D(cm^2/sec)$	$T(^oK)$	$D(cm^2/sec)$
1050	$2.60 \cdot 10^{-9}$	1372	$7.80 \cdot 10^{-9}$
1076	$8.00 \cdot 10^{-9}$	1395	$1.40 \cdot 10^{-8}$
1083	$6.10 \cdot 10^{-9}$	1437	$1.20 \cdot 10^{-8}$
1111	$9.80 \cdot 10^{-9}$	1443	$1.60 \cdot 10^{-8}$
1133	$1.10 \cdot 10^{-8}$	1538	$2.30 \cdot 10^{-8}$
1155	$1.60 \cdot 10^{-8}$	1560	$2.70 \cdot 10^{-8}$
		1582	$1.90 \cdot 10^{-8}$
1167	$5.20 \cdot 10^{-9}$	1616	$2.80 \cdot 10^{-8}$
1227	$5.40 \cdot 10^{-9}$	1667	$2.60 \cdot 10^{-8}$
1261	$6.30 \cdot 10^{-9}$	1695	$2.80 \cdot 10^{-8}$
1366	$7.80 \cdot 10^{-9}$	1783	$3.10 \cdot 10^{-8}$
		1789	$4.30 \cdot 10^{-8}$

TABLE IV CONCLUDED

Cs-133

$T(^{o}K)$	$D(cm^2/sec)$	$T(^{o}K)$	$D(cm^2/sec)$
992	$4.46 \cdot 10^{-9}$	1377	$1.09 \cdot 10^{-8}$
1040	$5.50 \cdot 10^{-9}$	1393	$9.96 \cdot 10^{-9}$
1070	$7.32 \cdot 10^{-9}$	1422	$1.20 \cdot 10^{-8}$
1082	$7.96 \cdot 10^{-9}$	1506	$1.54 \cdot 10^{-8}$
1100	$9.58 \cdot 10^{-9}$	1543	$1.59 \cdot 10^{-8}$
1122	$1.24 \cdot 10^{-8}$	1555	$2.20 \cdot 10^{-8}$
1124	$1.03 \cdot 10^{-8}$	1600	$1.58 \cdot 10^{-8}$
1133	$1.01 \cdot 10^{-8}$	1623	$2.14 \cdot 10^{-8}$
1181	$1.38 \cdot 10^{-8}$	1631	$1.75 \cdot 10^{-8}$
		1650	$1.61 \cdot 10^{-8}$
1178	$3.74 \cdot 10^{-9}$	1712	$1.78 \cdot 10^{-8}$
1289	$5.19 \cdot 10^{-9}$	1745	$2.47 \cdot 10^{-8}$
1316	$8.42 \cdot 10^{-9}$		
1326	$5.33 \cdot 10^{-9}$		
1366	$7.35 \cdot 10^{-9}$		

TABLE V

DIFFUSION COEFFICIENTS OF THE ALKALI METALS IN ZIRCALOY-2

Na-23

$T(^{o}K)$	$D(cm^2/sec)$	$T(^{o}K)$	$D(cm^2/sec)$
914	$5.67\cdot10^{-9}$	1135	$3.21\cdot10^{-9}$
933	$5.20\cdot10^{-9}$	1149	$4.42\cdot10^{-9}$
955	$1.10\cdot10^{-8}$	1157	$3.43\cdot10^{-9}$
991	$1.78\cdot10^{-8}$	1181	$7.61\cdot10^{-9}$
1013	$1.88\cdot10^{-8}$	1185	$7.66\cdot10^{-9}$
		1208	$8.11\cdot10^{-9}$
1060	$9.18\cdot10^{-10}$	1229	$9.51\cdot10^{-9}$
1075	$1.02\cdot10^{-9}$	1266	$1.86\cdot10^{-8}$
1076	$1.01\cdot10^{-9}$		
1091	$1.03\cdot10^{-9}$	1326	$5.30\cdot10^{-9}$
1117	$3.65\cdot10^{-9}$	1357	$1.23\cdot10^{-8}$
1121	$2.41\cdot10^{-9}$	1366	$2.03\cdot10^{-8}$

K-39

$T(^{o}K)$	$D(cm^2/sec)$	$T(^{o}K)$	$D(cm^2/sec)$
934	$1.10\cdot10^{-9}$	1122	$2.18\cdot10^{-9}$
939	$1.41\cdot10^{-9}$	1127	$4.33\cdot10^{-9}$
950	$2.06\cdot10^{-9}$	1129	$6.51\cdot10^{-9}$
956	$2.20\cdot10^{-9}$	1133	$2.70\cdot10^{-9}$
966	$2.63\cdot10^{-9}$	1140	$6.73\cdot10^{-9}$
982	$2.87\cdot10^{-9}$	1145	$6.61\cdot10^{-9}$
990	$5.03\cdot10^{-9}$	1181	$1.31\cdot10^{-8}$
990	$2.63\cdot10^{-9}$	1183	$1.00\cdot10^{-8}$
1002	$6.26\cdot10^{-9}$	1190	$1.16\cdot10^{-8}$
1008	$4.65\cdot10^{-9}$	1205	$1.71\cdot10^{-8}$
1013	$3.86\cdot10^{-9}$	1227	$2.25\cdot10^{-8}$
1022	$6.49\cdot10^{-9}$	1248	$2.67\cdot10^{-8}$
1026	$4.68\cdot10^{-9}$	1259	$2.59\cdot10^{-8}$
		1272	$4.39\cdot10^{-8}$
1066	$9.99\cdot10^{-10}$		
1073	$1.49\cdot10^{-9}$	1302	$1.34\cdot10^{-9}$
1076	$2.11\cdot10^{-9}$	1323	$2.96\cdot10^{-9}$
1083	$1.71\cdot10^{-9}$	1332	$4.60\cdot10^{-9}$
1087	$1.35\cdot10^{-9}$	1340	$6.70\cdot10^{-9}$
1096	$1.45\cdot10^{-9}$	1344	$6.79\cdot10^{-9}$
1101	$3.56\cdot10^{-9}$	1361	$9.79\cdot10^{-9}$
1111	$4.56\cdot10^{-9}$	1391	$2.11\cdot10^{-8}$

TABLE V CONCLUDED

Rb-85				Cs-133			
$T(^oK)$	$D(cm^2/sec)$	$T(^oK)$	$D(cm^2/sec)$	$T(^oK)$	$D(cm^2/sec)$	$T(^oK)$	$D(cm^2/sec)$
917	$8.86 \cdot 10^{-10}$	1133	$3.50 \cdot 10^{-9}$	978	$1.83 \cdot 10^{-9}$	1139	$1.24 \cdot 10^{-8}$
941	$1.01 \cdot 10^{-9}$	1151	$3.63 \cdot 10^{-9}$	1010	$2.93 \cdot 10^{-9}$	1142	$1.46 \cdot 10^{-8}$
954	$1.84 \cdot 10^{-9}$	1174	$5.99 \cdot 10^{-9}$	1022	$3.87 \cdot 10^{-9}$	1149	$2.08 \cdot 10^{-8}$
973	$4.74 \cdot 10^{-9}$			1028	$8.23 \cdot 10^{-9}$	1160	$1.89 \cdot 10^{-8}$
990	$4.05 \cdot 10^{-9}$	1220	$2.76 \cdot 10^{-9}$	1044	$1.08 \cdot 10^{-8}$	1170	$1.76 \cdot 10^{-8}$
1008	$8.30 \cdot 10^{-9}$	1239	$3.30 \cdot 10^{-9}$	1050	$9.06 \cdot 10^{-9}$	1172	$1.78 \cdot 10^{-8}$
1020	$7.84 \cdot 10^{-9}$	1250	$2.71 \cdot 10^{-9}$			1186	$4.39 \cdot 10^{-8}$
1037	$1.04 \cdot 10^{-8}$	1267	$3.01 \cdot 10^{-9}$	1060	$4.26 \cdot 10^{-9}$	1193	$2.36 \cdot 10^{-8}$
		1267	$5.30 \cdot 10^{-9}$	1066	$6.51 \cdot 10^{-9}$	1205	$5.83 \cdot 10^{-8}$
1038	$1.52 \cdot 10^{-9}$	1284	$7.57 \cdot 10^{-9}$	1080	$8.78 \cdot 10^{-9}$	1222	$6.84 \cdot 10^{-8}$
1056	$1.39 \cdot 10^{-9}$	1294	$3.46 \cdot 10^{-9}$	1083	$5.20 \cdot 10^{-9}$	1252	$5.22 \cdot 10^{-8}$
1059	$2.57 \cdot 10^{-9}$	1300	$6.50 \cdot 10^{-9}$	1083	$1.11 \cdot 10^{-8}$		
1060	$2.42 \cdot 10^{-9}$	1326	$5.01 \cdot 10^{-9}$	1094	$1.16 \cdot 10^{-8}$	1305	$9.67 \cdot 10^{-9}$
1087	$2.73 \cdot 10^{-9}$	1330	$8.22 \cdot 10^{-9}$	1100	$7.88 \cdot 10^{-9}$	1311	$8.52 \cdot 10^{-9}$
1107	$2.30 \cdot 10^{-9}$	1332	$9.38 \cdot 10^{-9}$	1111	$7.85 \cdot 10^{-9}$	1344	$1.77 \cdot 10^{-8}$
1107	$2.61 \cdot 10^{-9}$	1462	$2.20 \cdot 10^{-8}$	1116	$1.21 \cdot 10^{-8}$	1370	$1.63 \cdot 10^{-8}$
1122	$3.60 \cdot 10^{-9}$	1511	$6.35 \cdot 10^{-8}$	1122	$1.63 \cdot 10^{-8}$	1395	$2.25 \cdot 10^{-8}$
				1136	$1.86 \cdot 10^{-8}$		

TABLE VI

DIFFUSION COEFFICIENTS OF THE ALKALI METALS IN 304 STAINLESS STEEL

Li-7

$T(^{\circ}K)$	$D(cm^2/sec)$	$T(^{\circ}K)$	$D(cm^2/sec)$
1140	$5.57 \cdot 10^{-10}$	1289	$1.30 \cdot 10^{-9}$
1143	$5.81 \cdot 10^{-10}$	1316	$1.55 \cdot 10^{-9}$
1156	$1.11 \cdot 10^{-9}$	1319	$1.97 \cdot 10^{-9}$
1175	$1.63 \cdot 10^{-9}$	1340	$3.78 \cdot 10^{-9}$
1186	$1.62 \cdot 10^{-9}$	1344	$4.22 \cdot 10^{-9}$
1189	$2.06 \cdot 10^{-9}$	1368	$8.23 \cdot 10^{-9}$
1220	$3.35 \cdot 10^{-9}$	1379	$6.76 \cdot 10^{-9}$
		1427	$2.71 \cdot 10^{-8}$

Na-23

$T(^{\circ}K)$	$D(cm^2/sec)$	$T(^{\circ}K)$	$D(cm^2/sec)$
948	$3.85 \cdot 10^{-10}$	1208	$1.69 \cdot 10^{-9}$
983	$3.58 \cdot 10^{-10}$		
1002	$5.29 \cdot 10^{-10}$	1227	$1.37 \cdot 10^{-9}$
1044	$6.11 \cdot 10^{-10}$	1239	$1.17 \cdot 10^{-9}$
1106	$1.15 \cdot 10^{-9}$	1241	$2.19 \cdot 10^{-9}$
1122	$1.09 \cdot 10^{-9}$	1272	$4.63 \cdot 10^{-9}$
1133	$1.19 \cdot 10^{-9}$	1276	$5.54 \cdot 10^{-9}$
1149	$1.35 \cdot 10^{-9}$	1326	$1.07 \cdot 10^{-8}$
1168	$1.19 \cdot 10^{-9}$		

K-39

$T(^{\circ}K)$	$D(cm^2/sec)$	$T(^{\circ}K)$	$D(cm^2/sec)$
953	$4.51 \cdot 10^{-10}$	1119	$1.69 \cdot 10^{-9}$
986	$7.47 \cdot 10^{-10}$	1134	$1.82 \cdot 10^{-9}$
1008	$1.01 \cdot 10^{-9}$	1172	$2.26 \cdot 10^{-9}$
1038	$9.64 \cdot 10^{-10}$	1175	$2.21 \cdot 10^{-9}$
1040	$1.24 \cdot 10^{-9}$	1198	$2.56 \cdot 10^{-9}$
1050	$1.34 \cdot 10^{-9}$	1215	$2.75 \cdot 10^{-9}$
1062	$1.51 \cdot 10^{-9}$		
1073	$1.25 \cdot 10^{-9}$	1305	$5.34 \cdot 10^{-10}$
1075	$1.30 \cdot 10^{-9}$	1330	$8.73 \cdot 10^{-10}$
1076	$1.58 \cdot 10^{-9}$	1389	$3.06 \cdot 10^{-9}$
1109	$1.36 \cdot 10^{-9}$	1433	$6.73 \cdot 10^{-9}$
1116	$2.21 \cdot 10^{-9}$		

Rb-85

$T(^{\circ}K)$	$D(cm^2/sec)$	$T(^{\circ}K)$	$D(cm^2/sec)$
1043	$6.28 \cdot 10^{-10}$	1161	$4.79 \cdot 10^{-9}$
1060	$8.51 \cdot 10^{-10}$	1176	$4.53 \cdot 10^{-9}$
1065	$5.19 \cdot 10^{-10}$	1182	$6.78 \cdot 10^{-9}$
1071	$1.49 \cdot 10^{-9}$	1198	$9.27 \cdot 10^{-9}$
1080	$1.27 \cdot 10^{-9}$		
1116	$3.58 \cdot 10^{-9}$	1355	$1.13 \cdot 10^{-9}$
1127	$1.94 \cdot 10^{-9}$	1404	$3.01 \cdot 10^{-9}$
1133	$2.30 \cdot 10^{-9}$	1445	$1.11 \cdot 10^{-8}$
1155	$4.46 \cdot 10^{-9}$		

TABLE VI CONCLUDED

Cs-133

$T(^oK)$	$D(cm^2/sec)$	$T(^oK)$	$D(cm^2/sec)$
960	$1.52 \cdot 10^{-9}$	1166	$1.23 \cdot 10^{-8}$
962	$1.22 \cdot 10^{-9}$	1175	$1.24 \cdot 10^{-8}$
975	$2.15 \cdot 10^{-9}$	1195	$1.39 \cdot 10^{-8}$
1016	$2.37 \cdot 10^{-9}$	1200	$2.10 \cdot 10^{-8}$
1038	$3.76 \cdot 10^{-9}$	1205	$2.15 \cdot 10^{-8}$
1041	$4.03 \cdot 10^{-9}$		
1055	$5.78 \cdot 10^{-9}$	1287	$3.75 \cdot 10^{-9}$
1070	$3.79 \cdot 10^{-9}$	1379	$6.43 \cdot 10^{-9}$
1075	$6.19 \cdot 10^{-9}$	1381	$7.65 \cdot 10^{-9}$
1087	$6.79 \cdot 10^{-9}$	1412	$7.87 \cdot 10^{-9}$
1105	$6.09 \cdot 10^{-9}$	1427	$1.15 \cdot 10^{-8}$
1114	$1.39 \cdot 10^{-8}$	1431	$9.98 \cdot 10^{-9}$
1116	$9.42 \cdot 10^{-9}$	1439	$8.30 \cdot 10^{-9}$
1120	$1.31 \cdot 10^{-8}$	1443	$1.00 \cdot 10^{-8}$
1136	$1.16 \cdot 10^{-8}$	1484	$1.39 \cdot 10^{-8}$
1152	$1.66 \cdot 10^{-8}$		

Table VII

D_o and Q for IMPURITY DIFFUSION in 304 STAINLESS STEEL

$928 < T(^oK) < 1228$

Impurity	D_o	Q
Li-7	$(1.86 \pm 2.01) \times 10^0$	52.96 ± 0.54
Na-23	$(6.11 \pm 0.56) \times 10^{-7}$	14.22 ± 0.19
K-39	$(9.53 \pm 0.67) \times 10^{-7}$	14.09 ± 0.15
Rb-85	$(3.19 \pm 0.58) \times 10^{-1}$	41.92 ± 0.38
Cs-133	$(6.75 \pm 0.70) \times 10^{-4}$	25.04 ± 0.22

$1228 < T(^oK) < 1789$

Impurity	D_o	Q
Li-7	$(1.73 \pm 0.31) \times 10^5$	84.42 ± 0.56
Na-23	$(1.74 \pm 0.59) \times 10^4$	74.08 ± 0.93
K-39	$(1.72 \pm 0.10) \times 10^3$	75.22 ± 0.18
Rb-85	$(5.56 \pm 1.75) \times 10^6$	98.16 ± 1.01
Cs-133	$(5.03 \pm 0.49) \times 10^{-5}$	24.50 ± 0.26

D_o is in units of cm^2/sec

Q is in units of kcal/mole

Table VIII

D_o and Q for IMPURITY DIFFUSION in TANTALUM

$990 < T(^oK) < 1230$

Impurity	D_o	Q
Li-7	$(5.15 \pm 0.91) \times 10^{-5}$	20.29 ± 0.41
Na-23	$(2.07 \pm 0.27) \times 10^{-6}$	11.90 ± 0.37
K-39	$(2.71 \pm 0.50) \times 10^{-3}$	32.19 ± 0.43
Rb-85	$(1.22 \pm 0.37) \times 10^{-1}$	36.46 ± 0.72
Cs-133	$(8.53 \pm 0.61) \times 10^{-6}$	15.07 ± 0.16

$1230 < T(^oK) < 1790$

Impurity	D_o	Q
Li-7	$(3.38 \pm 0.35) \times 10^{-5}$	25.49 ± 0.32
Na-23	$(1.13 \pm 0.17) \times 10^{-6}$	15.46 ± 0.47
K-39	$(1.06 \pm 0.07) \times 10^{-5}$	22.25 ± 0.20
Rb-85	$(2.33 \pm 0.24) \times 10^{-7}$	14.78 ± 0.31
Cs-133	$(1.18 \pm 0.12) \times 10^{-6}$	13.48 ± 0.26

D_o is in units of cm^2/sec

Q is in units of kcal/mole

Table IX

D_o and Q for IMPURITY DIFFUSION in ZIRCALOY-2

$900 < T(^oK) < 1045$

Impurity	D_o	Q
Na-23	$(9.76 \pm 2.99) \times 10^{-3}$	26.44 ± 0.72
K-39	$(2.12 \pm 0.31) \times 10^{-2}$	30.92 ± 0.31
Rb-85	$(1.11 \pm 0.26) \times 10^{1}$	42.82 ± 0.55
Cs-133	$(8.91 \pm 2.96) \times 10^{2}$	52.91 ± 0.79

$1045 < T(^oK) < 1345$

Impurity	D_o	Q
Na-23	$(1.92 \pm 0.25) \times 10^{-1}$	40.77 ± 0.37
K-39	$(3.08 \pm 0.41) \times 10^{0}$	46.10 ± 0.38
Rb-85	$(3.53 \pm 0.54) \times 10^{-4}$	25.79 ± 0.44
Cs-133	$(7.74 \pm 1.01) \times 10^{-2}$	35.03 ± 0.37

$1345 < T(^oK) < 1520$

Impurity	D_o	Q
Na-23	$(5.46 \pm 0.75) \times 10^{10}$	116.19 ± 3.48
K-39	$(5.35 \pm 0.82) \times 10^{9}$	111.06 ± 0.58
Rb-85	$(1.11 \pm 0.22) \times 10^{-2}$	37.59 ± 0.75
Cs-133	$(1.21 \pm 0.30) \times 10^{-2}$	36.74 ± 0.94

D_o is in units of cm^2/sec

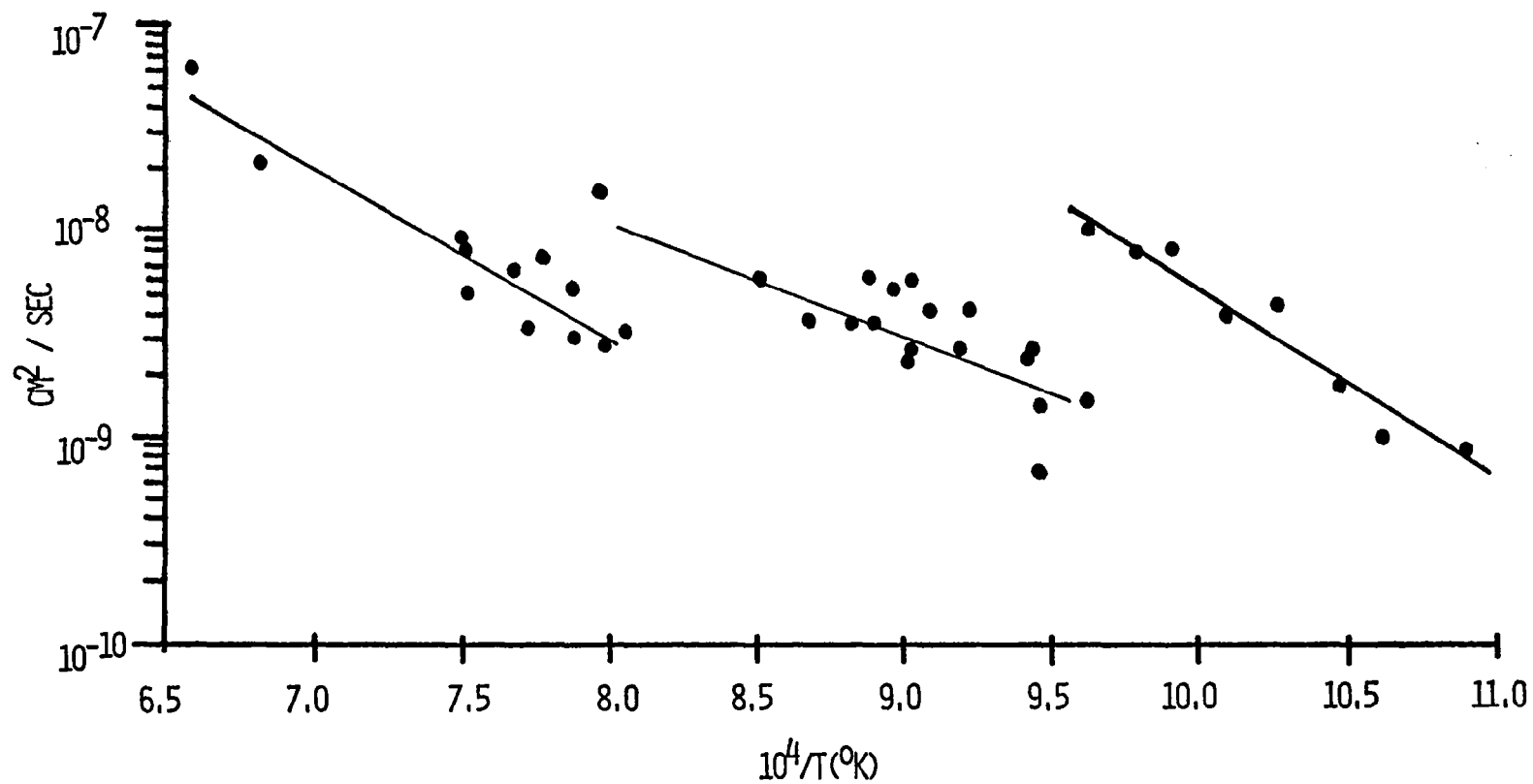Q is in units of kcal/mole
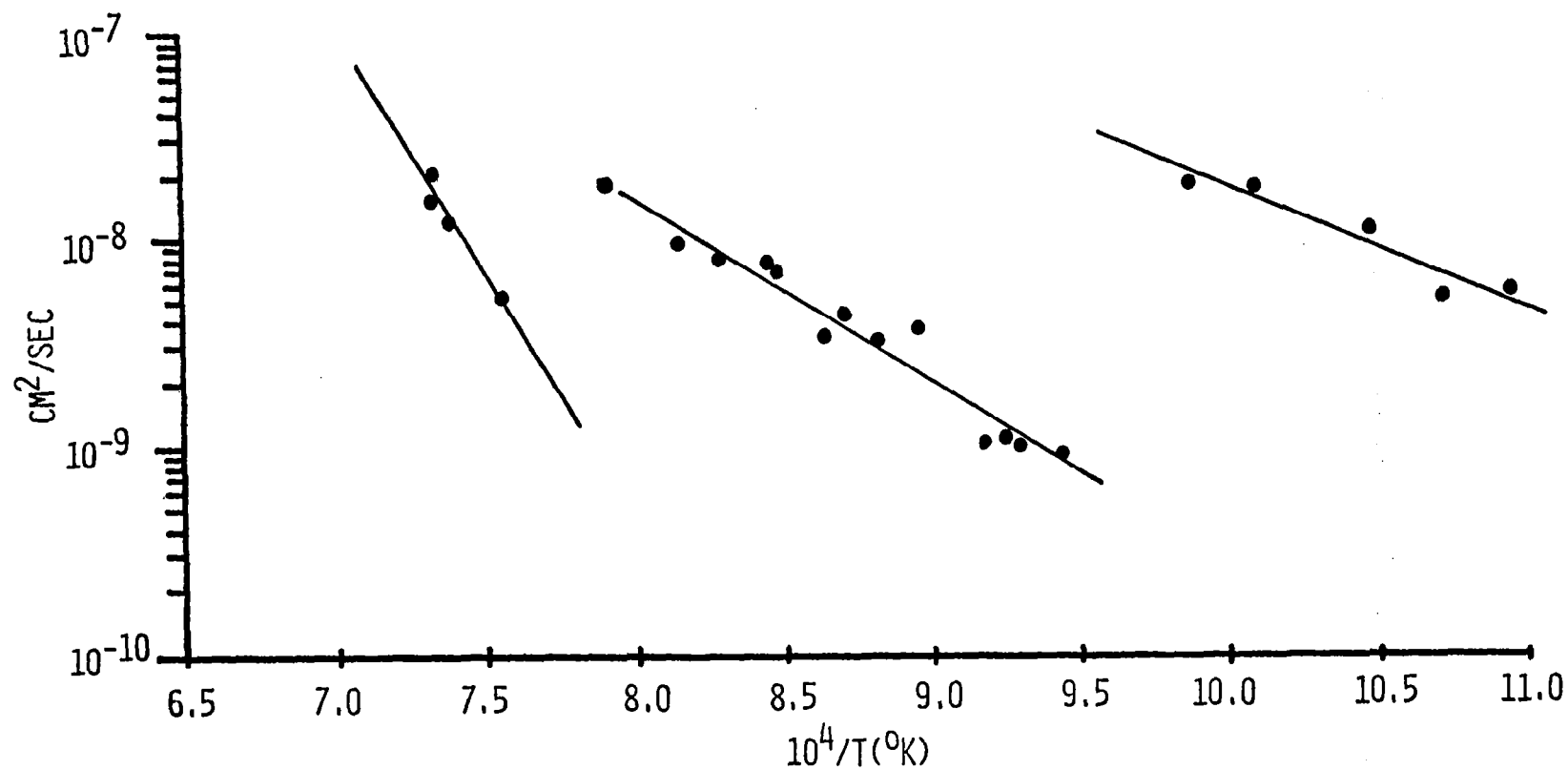
ACTIVATION ENERGY DIAGRAM OF Na-23 IN ZIRCALOY II
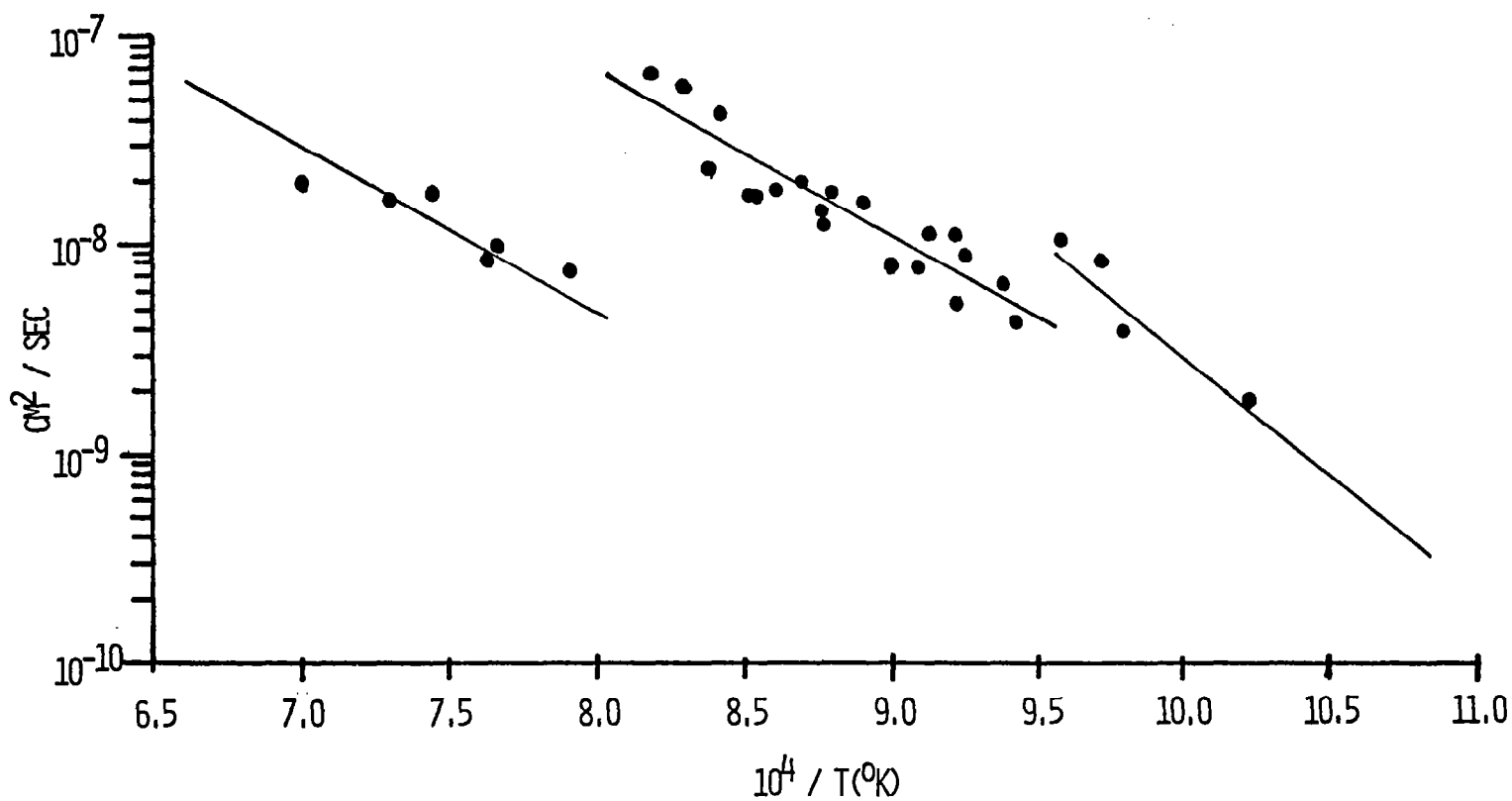
Figure 7

99
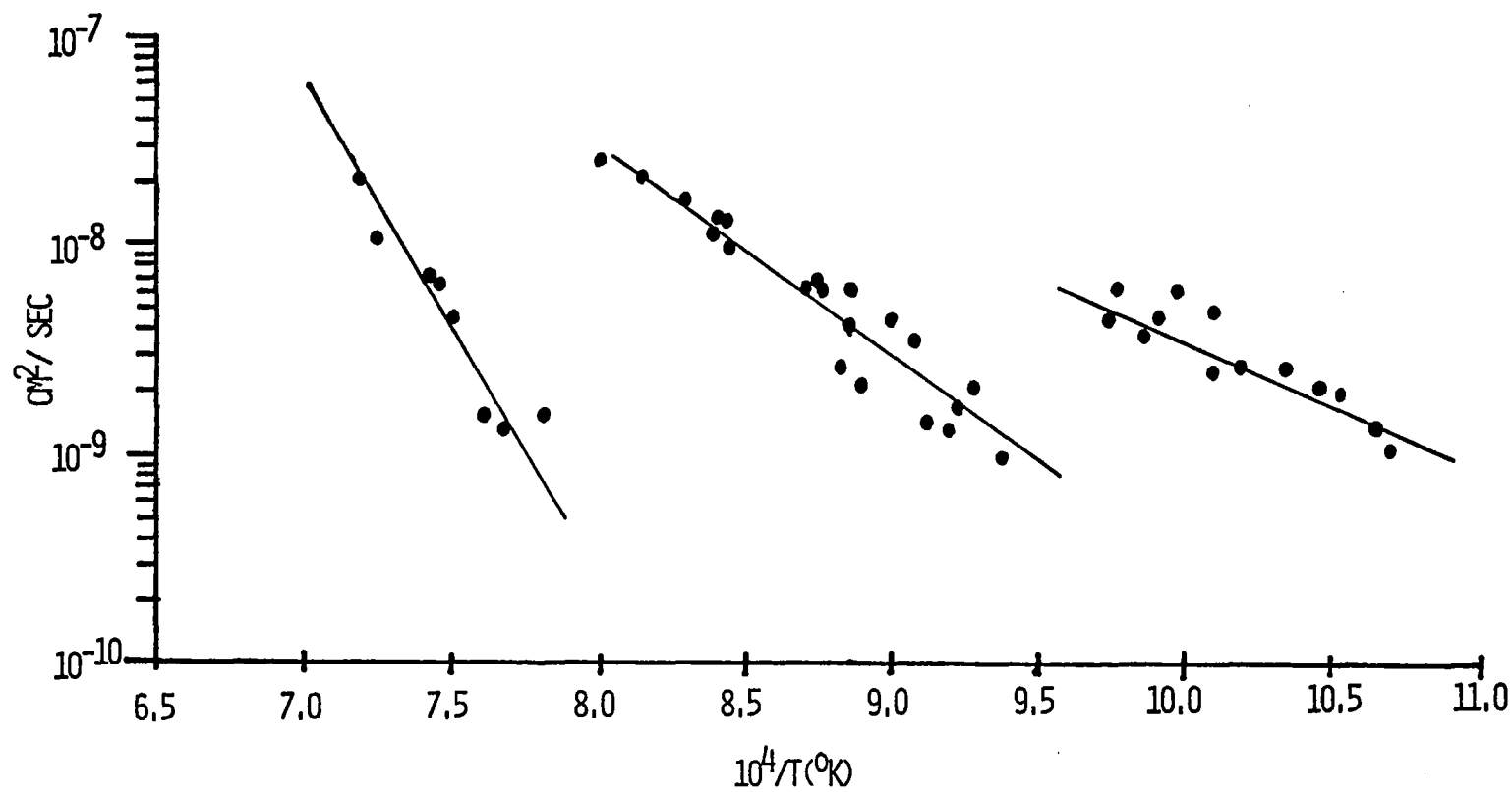
ACTIVATION ENERGY DIAGRAM OF K-39 IN ZIRCALOY-II
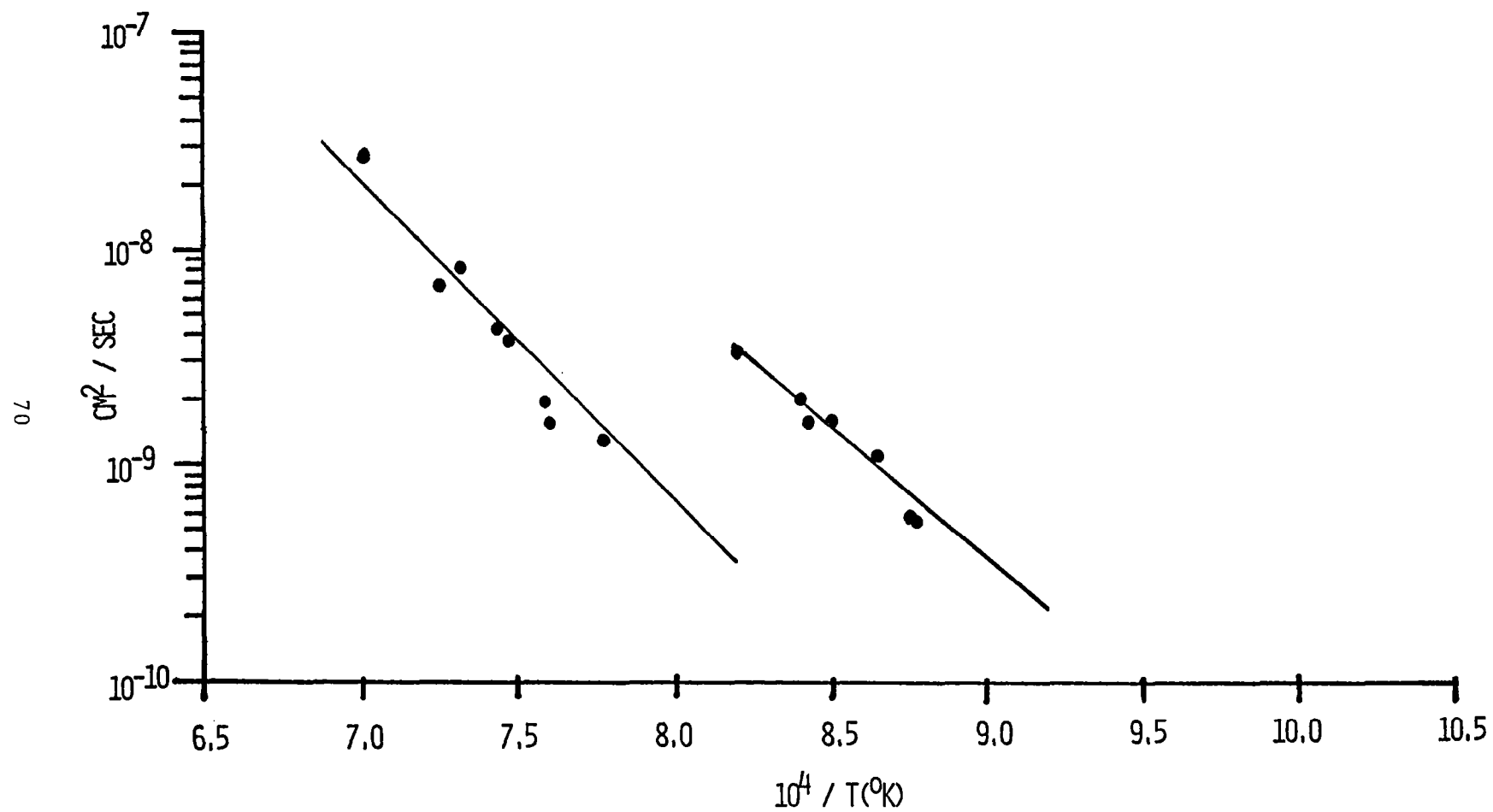
Figure 8

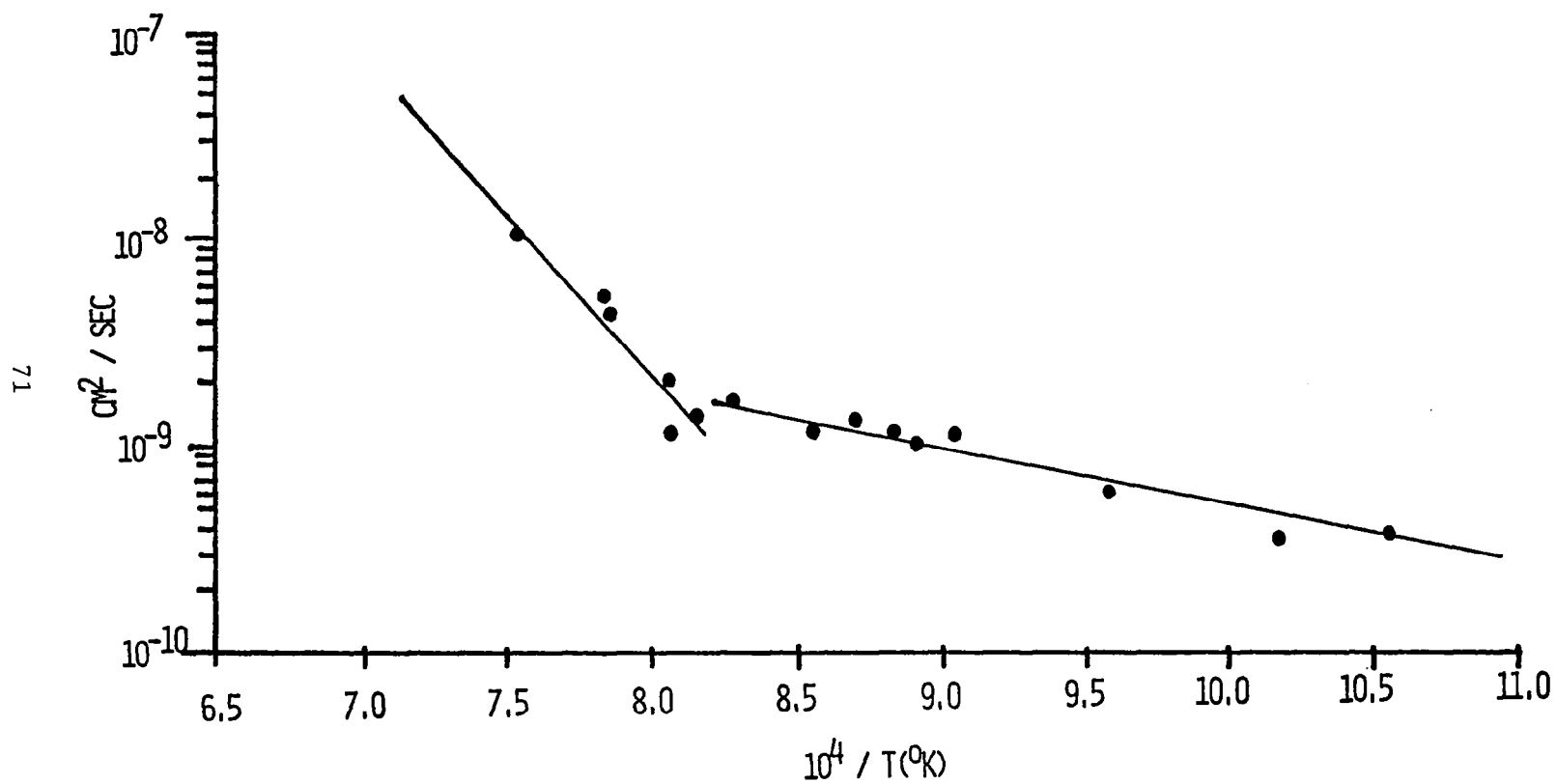ACTIVATION ENERGY DIAGRAM OF RB-85 IN ZIRCALOY-II

Figure 9

89

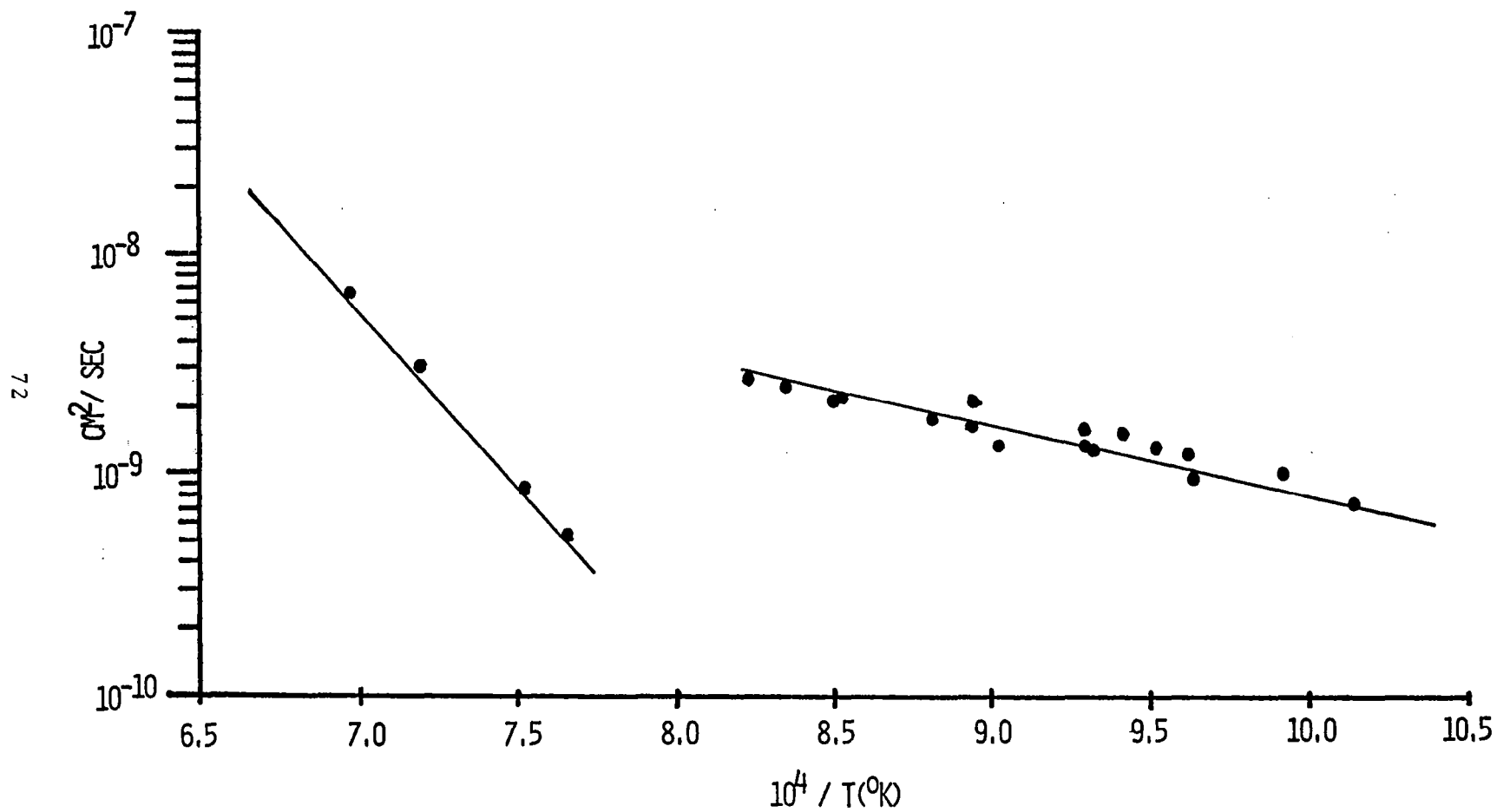ACTIVATION ENERGY DIAGRAM OF Cs-133 IN ZIRCALOY-II

Figure 10

ACTIVATION ENERGY DIAGRAM OF Li-7 IN 304 STAINLESS STEEL
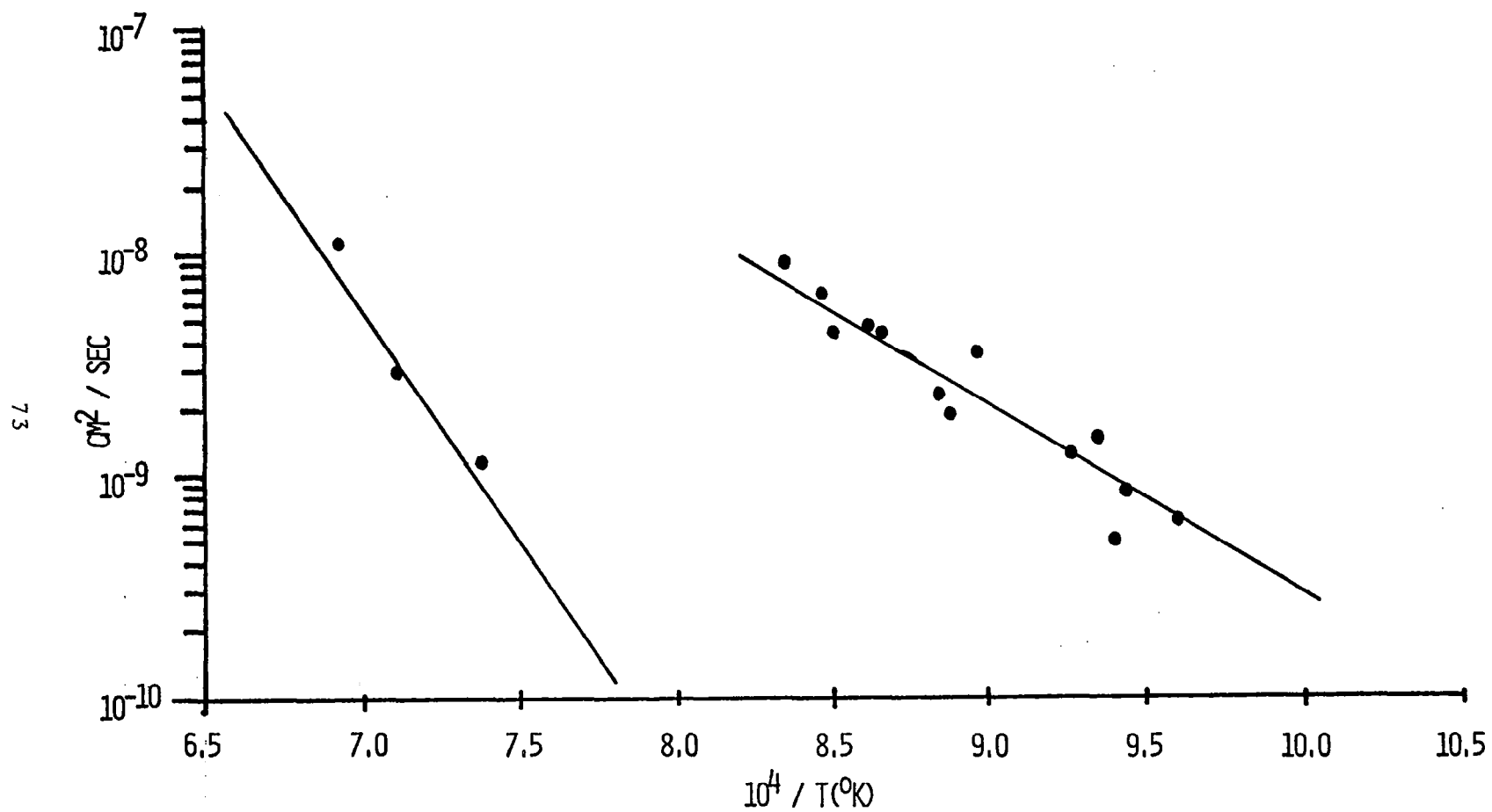
Figure 11

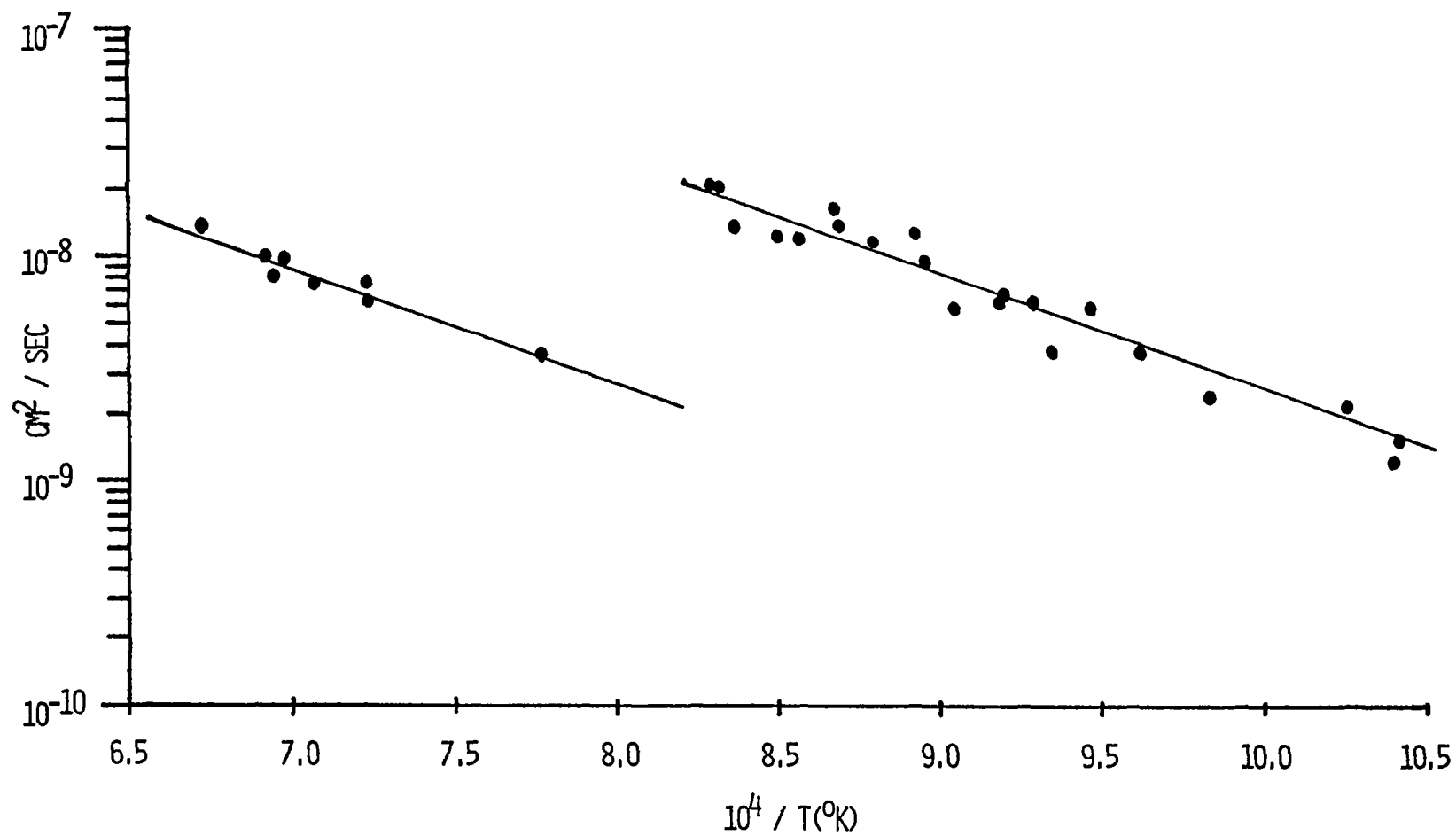ACTIVATION ENERGY DIAGRAM OF Na-23 IN 304 STAINLESS STEEL

Figure 12

ACTIVATION ENERGY DIAGRAM OF K-39 IN 304 STAINLESS STEEL

Figure 13

ACTIVATION ENERGY DIAGRAM OF Rв-85 IN 304 STAINLESS STEEL

Figure 14

73

ACTIVATION ENERGY DIAGRAM OF Cs-133 IN 304 STAINLESS STEEL

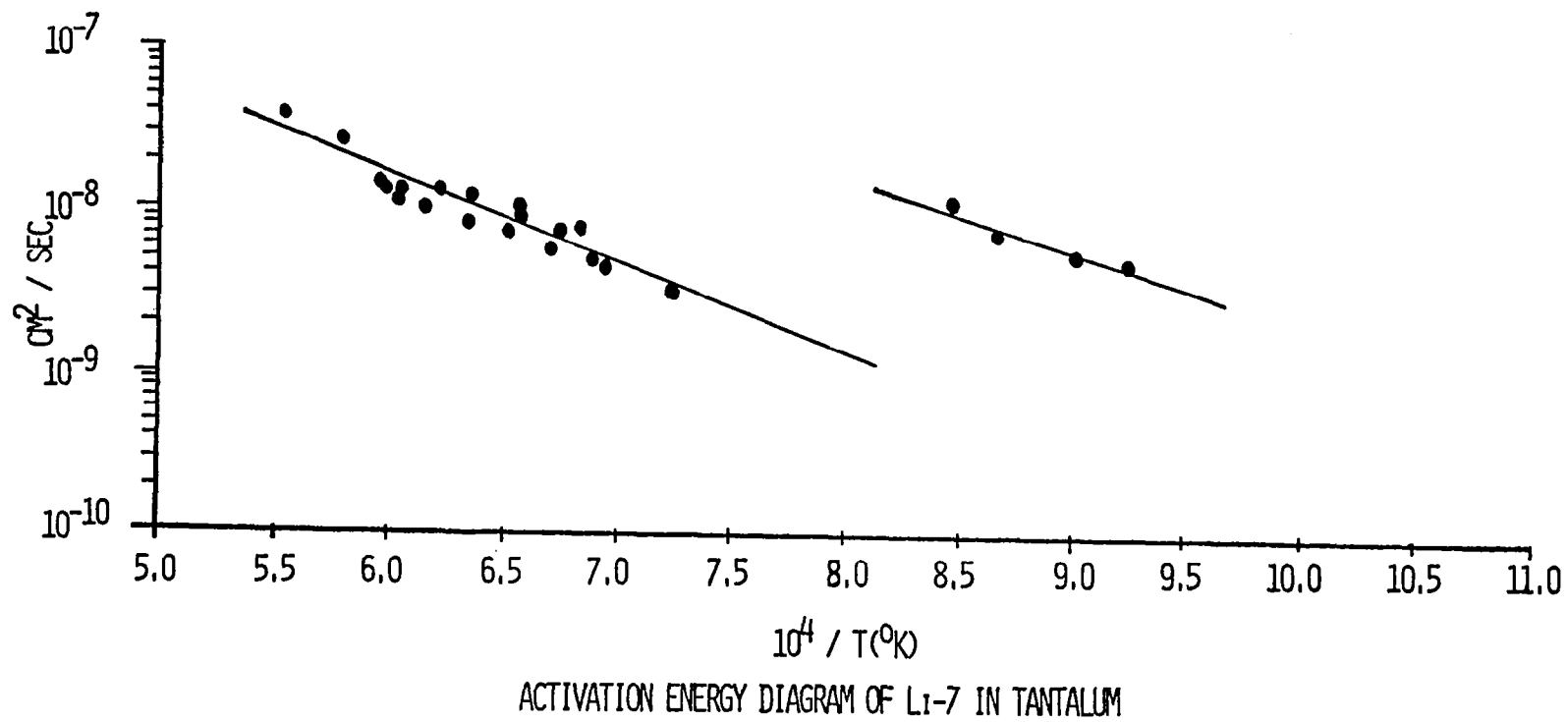Figure 15

74

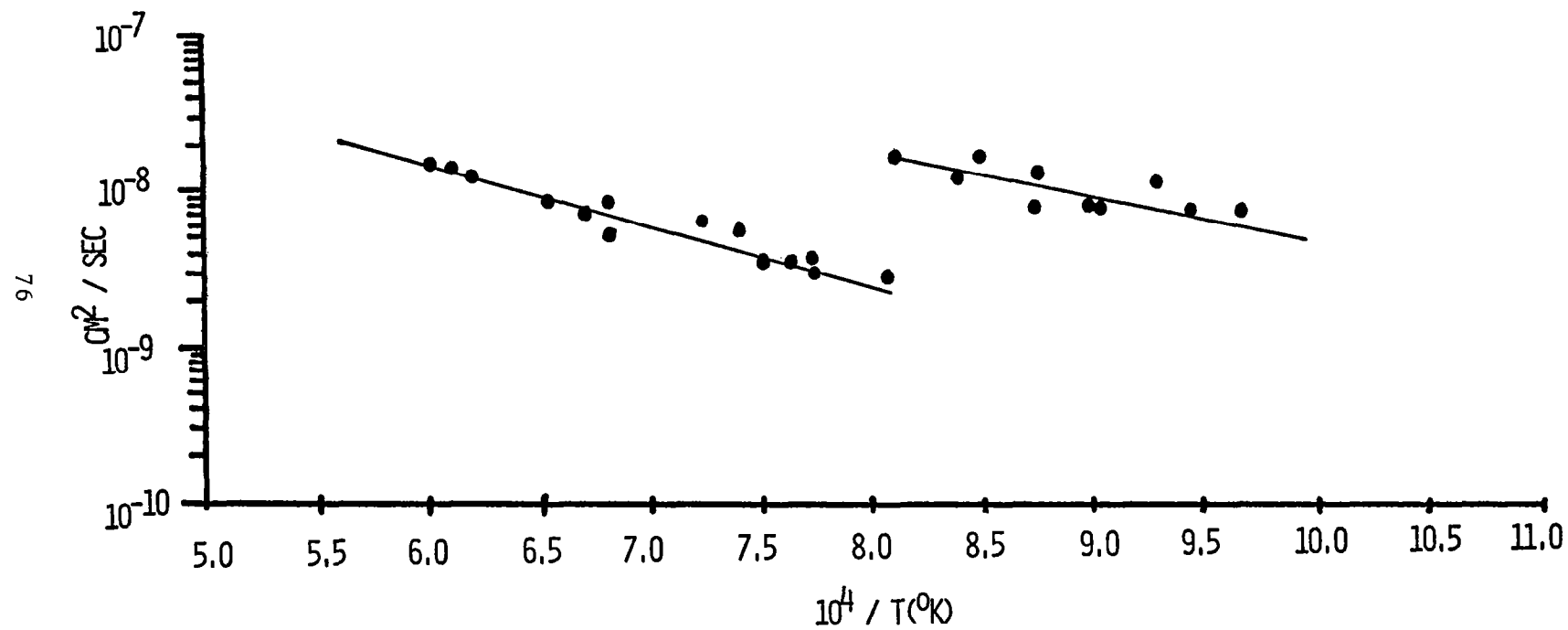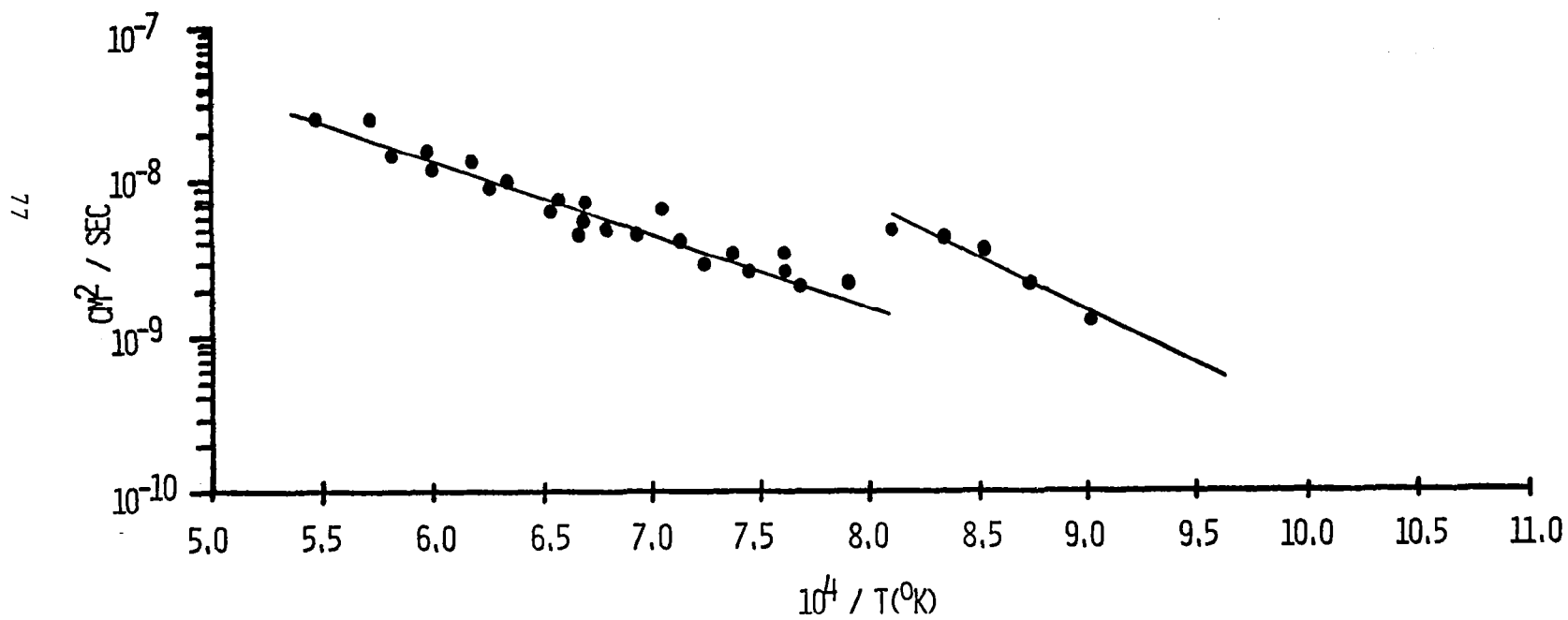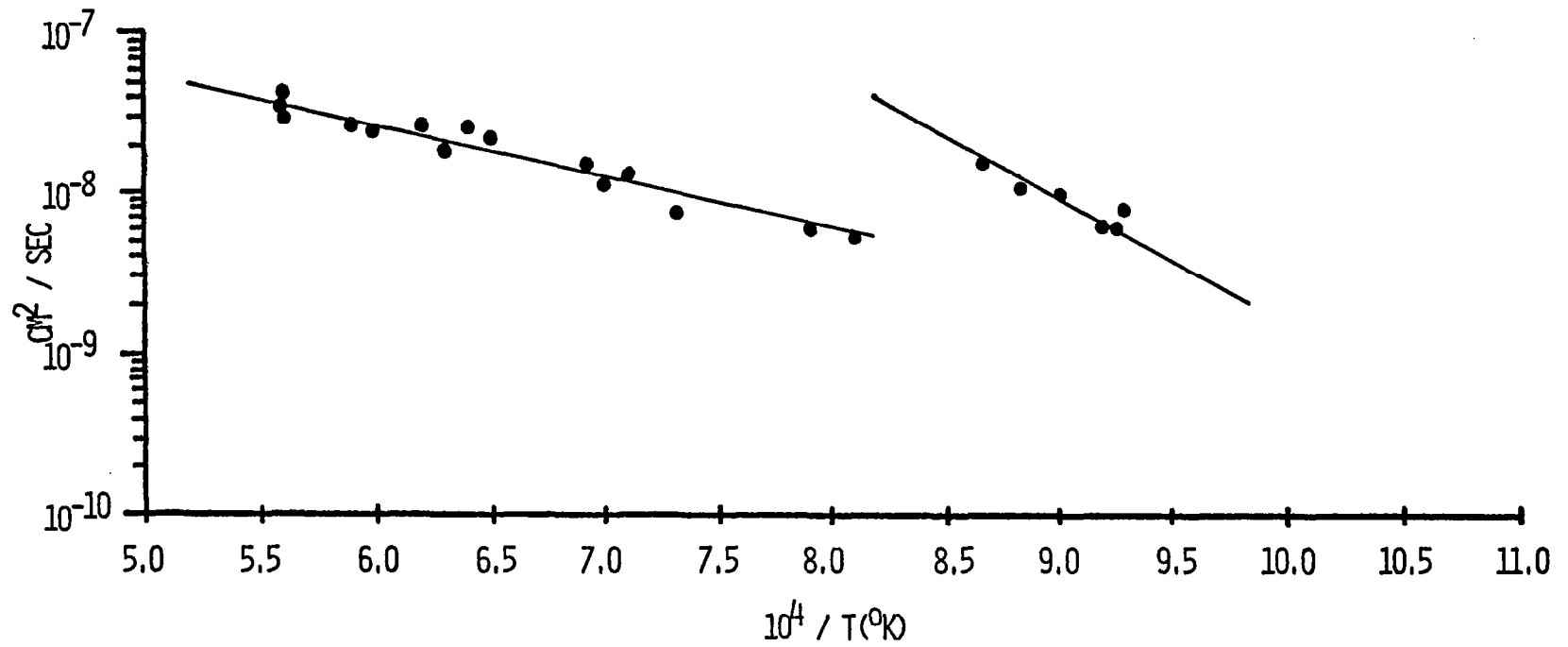ACTIVATION ENERGY DIAGRAM OF Lɪ-7 IN TANTALUM

Figure 16

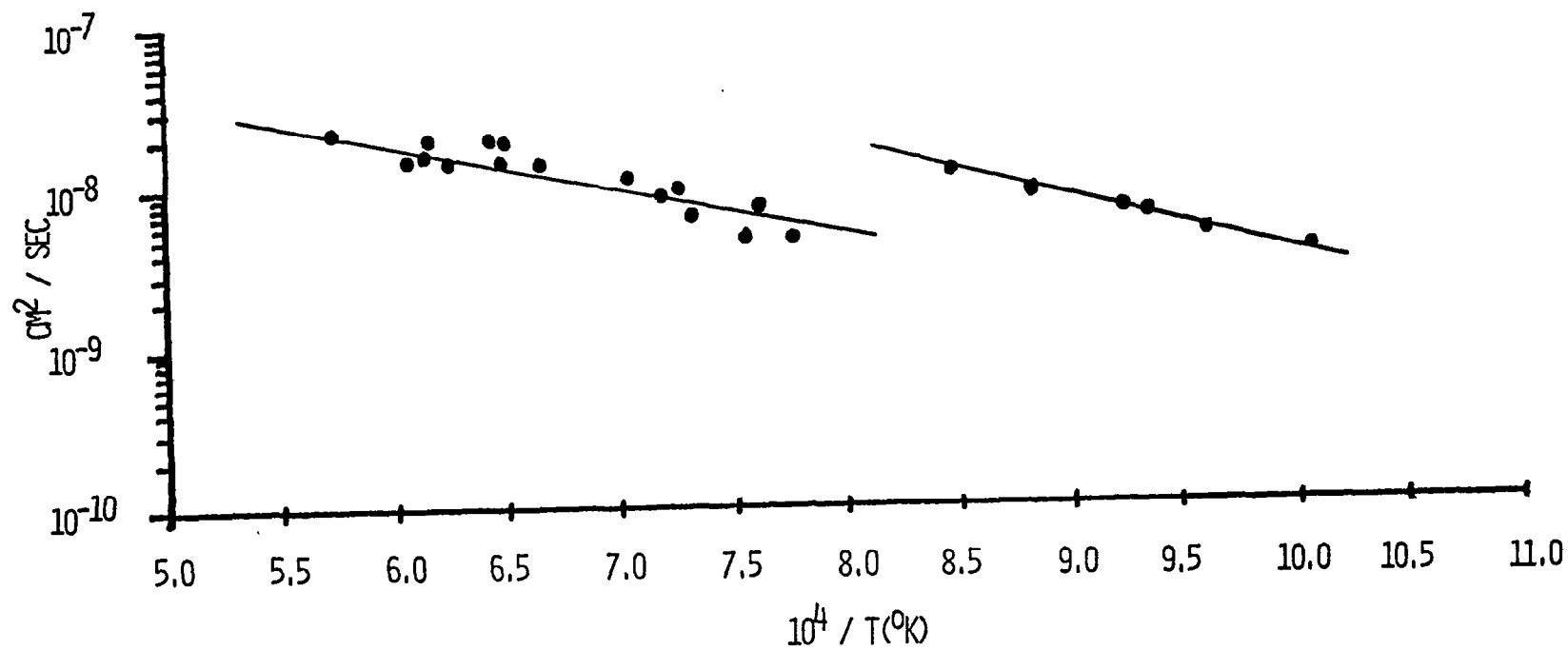ACTIVATION ENERGY DIAGRAM OF Na-23 IN TANTALUM

Figure 17

ACTIVATION ENERGY DIAGRAM OF K-39 IN TANTALUM

Figure 18

ACTIVATION ENERGY DIAGRAM OF Rʙ-85 IN TANTALUM

Figure 19

ACTIVATION ENERGY DIAGRAM OF Cs-133 IN TANTALUM

Figure 20

both a hexagonal close packed, h.c.p., and a body centered cubic, b.c.c., geometry depending on the temperature, zircaloy-2, which has a composition of ~98.5% zirconium, will probably have a h.c.p. and b.c.c. structure. However, instead of having a single discontinuity, there is a large transition region which possesses its own diffusion characteristics. Pande, Naik, and Agarwala[43] have also observed this three region activation energy diagram in their study of the diffusion of chromium and iron in zircaloy-2. Their transition region held limits of 780 and 980°C, while this work extends the transition region from 772 to 1072°C. This large transition region can be explained by a statistical average of the diffusivity of both phases present at a particular temperature

When examining the stainless, steels, the results in this work did not completely agree with literature values. A reason for the discrepancy may involve the fact that the composition of stainless steel has a wide range in the percent abundance of its constituent elements. For example, Delong[44] has found that 304 stainless steel changes from a face centered cubic, f.c.c., to a body centered cubic, b.c.c., structure at 910°C, while the results in this study indicate a phase change at 955°C.

While carbon,[45] deuterium and hydrogen,[46] molybdenum,[47] and sulpher[48] have been studied as they diffused through tantalum the diffusion of the alkali metals have not been studied in tantalum. Tantalum has a body centered cubic

structure, thus there will be no phase transformation. However, from the data obtained in this experiment it appears that there has been a phenomenological occurence at approximately $1000^{\circ}C$. There have been many possible explanations suggested, but the one that presents the greatest problem in discounting it is that of cold working. For tantalum to be processed into the thin ribbons used in this study, tantalum would undergo a great deal of cold working. It is possible to remove these defects by annealing, and it so happens that the annealing temperature for tantalum is $1000^{\circ}C$. The resultant reduction in lattice disorder would tend to decrease the diffusion coefficient. However, it would increase when the temperature was again increased. This is exactly what occurs in figures 16 - 20.

These results provide an insight into the basic diffusion mechanism in addition to supplying D, D_o, and Q. For example, the relationship between the diffusion coefficient, D, and the ionic radius at a constant temperature can be compared, by considering the alkali metal series; Li, Na, K, Rb, and Cs, in the same host material. Plots of these five impurity ions as observed in this study are shown in Figure 21 for tantalum, Figure 22 for zircaloy-2, and Figure 23 for 304 stainless steel. Although there is no phenomenalogical relationship, the diffusion coefficient versus mass is somewhat analoguous to sputtering yield data in which very large differences in secondary ion yield vary with atomic mass and ionic radius.

Each set of figures must be considered separately, as they represent completely different crystalline structures and alloy compositions.

Tantalum: Referring to Figure 21 A and B, there is a similarity in the pattern of the constant temperature lines. Independent of the ambient temperature of the material, the diffusion coefficient seems to follow the same pattern of maxima and minima with increasing ionic radius. Similar diffusion patterns can be expected if there were no changed in either/or both the diffusion mechanism and the geometric structure of the crystal. There has been no reported phase change in tantalum, which always possesses body centered cubic geometry. Note that as both the ionic radius of the impurity, r_{imp}(Å), and T(^{o}K) increase, there appears to be an upper limit on the order of 10^{-8} cm^{2}/sec for D. At the same time there is a "collimating" effect on D as r_{imp} goes from approximately 1Å to approximately 1.33Å. In an attempt to determine the reason for the behavior at these two points, an intersititial mechanism for diffusion was assumed and the largest sized impurity which would fit through the confining lattice ions for a b.c.c. system was calculated. For a b.c.c. system the following formula was used

$$r_{impurity\ ion} < a/\sqrt{2} - r_{lattice\ ion} \tag{59}$$

where a is the edge size. For tantalum, it was found that r_{imp} should be less than 1.66 Å. This is extremely close to

$$D(\text{CM}^2/\text{SEC}) \text{ VS } r_{imp}(\overset{o}{A}) \text{ AT CONSTANT } T(^o K) \text{ IN TANTALUM}$$
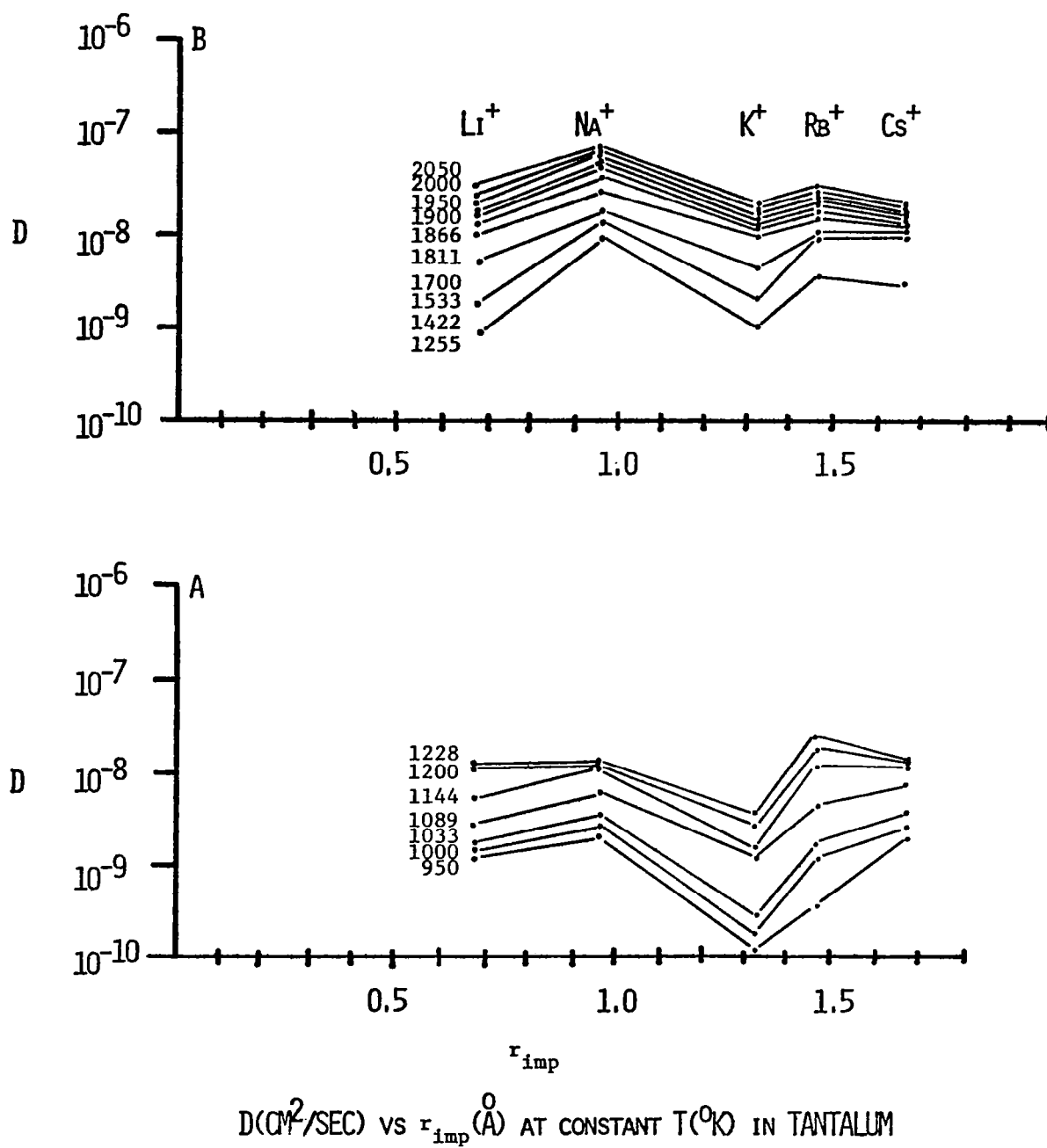
Figure 21

83

the 1.67 Å point on the graph for the Cs^+ ion. This implies
that the lattice structure of the host material plays a role
in limiting the size of the impurity ion's diffusion. To
go beyond this size would require additional energy. The
region of $1 < r_{imp}(Å) < 1.33$ shows what might be considered
inhibited diffusion. This could be caused by the simultane-
ous diffusion of all the other impurities in this dynamic
system while being analyzed for just one particular impurity.

Zircaloy-2: A very interesting pattern of diffusion
can be observed in Figures 22 A, B, and C. Using the $900°K$
line in Fig. 22 A as a reference, in a h.c.p. structure, as
the ionic radius of the impurity increases, the diffusion co-
efficient decreases. However, as the temperature is increased
it is evident that the lattice vibrations cause D to increase
and the larger impurity ions to diffuse at a greater rate.
This increase in acceptable ionic radius appears to have an
upper limit of about 1.47 Å which corresponds closely to the
radius of the Rb^+ ion.

Figure 22 B represents the transition region where
the crystal structure changes from h.c.p. to b.c.c.. This
graph is not simply understood as the crystal structure
changes with temperature. It does appear that the disorder
induced in the crystal by the phase change increases the
probability of diffusion.

Figure 22 C shows the zircaloy-2 system in its b.c.c.
state. Note that $D(1250°K)$ is less than $D(1040°K)$ even though
the temperature has been increased into the higher temperature

phase region. A possible mechanism to qualitatively explain this sudden drop in diffusion rate is that as the transition region is approached from a lower temperature, lattice defects begin to occur before the transition point is actually reached. These lattice defects are greatly multiplied in number in the phase transition region due to the increased disorder in the lattice structure. This increases the impurity diffusion rate in the phase transition region. However, once the phase transition is passed, the crystal lattice became more ordered, and many of the lattice defects retreat to defect "sinks," such as grain boundaries. This results in an initial decrease in the diffusion rate. As the defect sinks will release these defects into the crystal lattice as the temperature increases, the diffusion rate will again begin to increase.

Figure 22 C shows an interesting occurrence as both $T(^{O}K)$ and $r_{imp}(\overset{O}{A})$ increase. In the region $r_{imp} > 1.47 \overset{O}{A}$, D is not only relatively invariant as r_{imp} increases, but also relatively invariant as the temperature increases. It seems that as T increases D is constrained to be of the order of magnitude of $10^{-8} cm^2/sec$. A partial explanation is proposed: if it is assumed that the solute will diffuse by an interstitial mechanism, a relationship for the largest impurity ion accepted before configuration problems are encountered is again equation (59). Using $r_{lattice\ ion}$ of zirconium, it is determined that $r_{imp} < 1.47 \overset{O}{A}$. From $r_{imp} = 1.47 \overset{O}{A}$ in Figure 22C, the diffusion coefficient changes very little
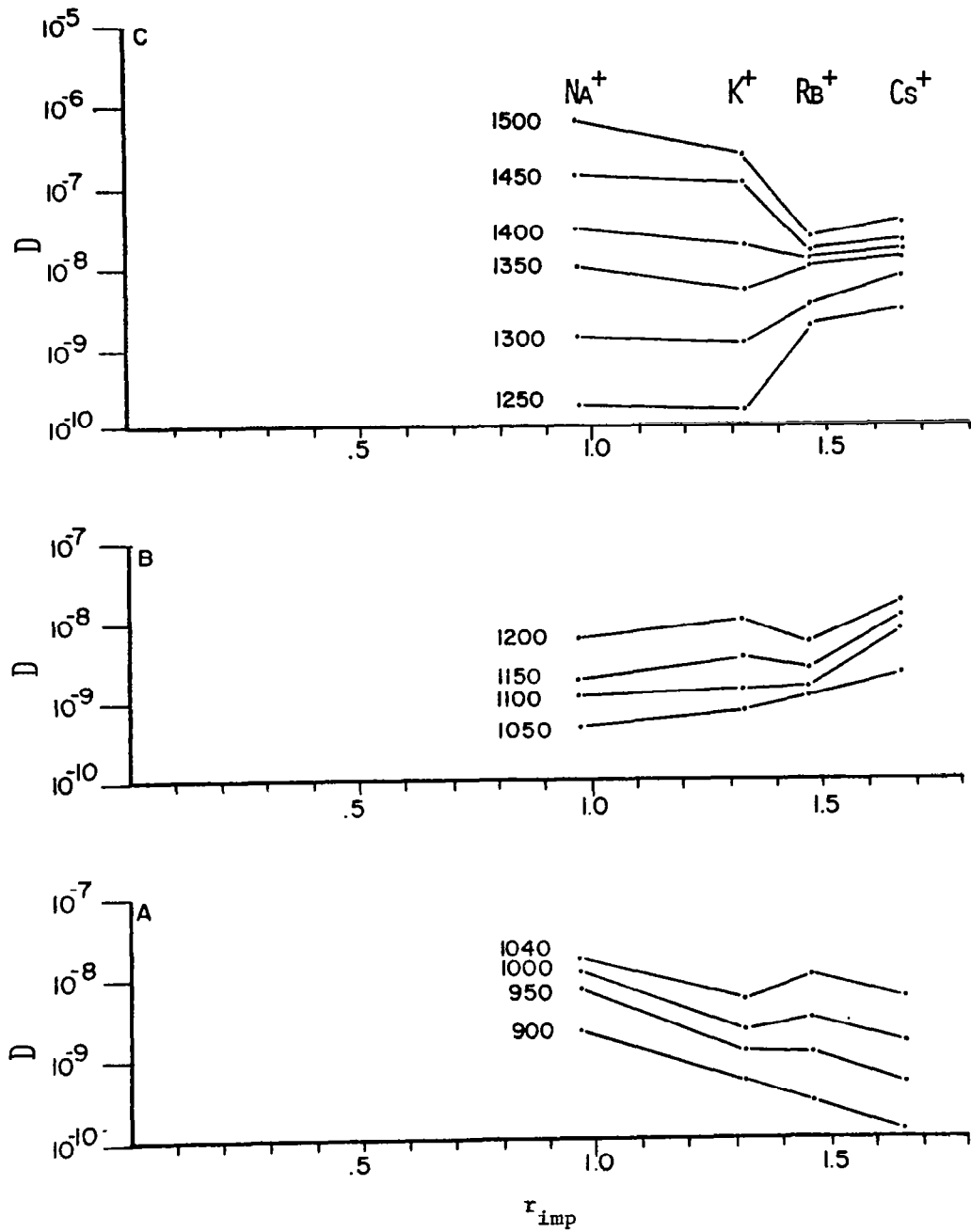
D(CM^2/SEC) vs r_{imp}(Å) AT CONSTANT T(°K) IN ZIRCALOY-II

Figure 22

86

with increasing r_{imp}. Even increasing the temperature does
not cause much of an increase in D after r_{imp} reaches 1.47 $\overset{o}{A}$.

The changing behavior of D in the range of 1.33
< $r_{imp}(\overset{o}{A})$ < 1.47 could possibly be explained by the fact that
the zircaloy-2 has a certain percentage (~1.5) of tin, which
has an ionic radius of 0.93 $\overset{o}{A}$. This means that for a given dif-
fusion jump through four restraining lattice ions, if one is
a tin ion, impurity ions of larger size will be able to dif-
fuse through easier than if all four lattice ions were zir-
conium. This would represent only a minor perturbation as
the amount of tin is limited. At higher temperatures, this
represents a negligible effect as r_{imp} gets closer to 1.47 $\overset{o}{A}$
the size plays an increasingly inhibiting effect.

304 Stainless Steel: Stainless steel 304 presents a
special challenge for determining diffusion parameters using
a mass spectrometer. No longer is just a pure metal being
considered, as in the case with tantalum, or a very dilute
alloy as with zircaloy-2, but an alloy which has major con-
stituents of iron, nickel and chromium. The activation energy
plots have shown the phase change representing a transforma-
tion from f.c.c. to b.c.c. along with the corresponding
activation energies. On the other hand, Figures 23 A and B
represent a more complex picture in regard to D as both, r_{imp}
and T are varied.

Figure 23 A represents the f.c.c. structure of the
stainless steel. As each succeeding temperature line is
examined, a pattern in the region of approximately 0.70 $\overset{o}{A}$

and 1.5 $\overset{o}{A}$ takes place with an apparent change of slope and vortex, respectively. This can be explained by the fact that as the temperature is increased the lattice vibrations are increased so that it is easier for the impurity of a larger size to diffuse. There is a limit as to the size that will be accommodated. This is primarily controlled by the crystallographic structure of the host lattice. Stainless steel is affected in that there may be unit cells of different host ions, representing the major constituents of stainless steel, and grain boundaries may differ for specific samples. When the effect of Ni in the f.c.c. structure is considered r_{imp} should be less than 1.07 $\overset{o}{A}$. Configurational limitations do not appear to be significant until r_{imp} is approximately 1.30 $\overset{o}{A}$ and that the region from 1.0 $\overset{o}{A}$ to 1.3 $\overset{o}{A}$ is a relatively temperature and radius independent region. When r_{imp} becomes greater than 1.33 $\overset{o}{A}$, the larger size ion cannot diffuse as readily until more energy is supplied to increase the lattice vibrations.

Figure 23 B represents the b.c.c. structure of 304 stainless steel where there are again inflection points which indicate an area of physical constraints. The point ~1 $\overset{o}{A}$ is caused by the influence of Ni, while the area around 1.3 $\overset{o}{A}$ is caused by the influence of Cr (r_{imp} should be less than 1.23 $\overset{o}{A}$) and Fe (r_{imp} should be less than 1.34 $\overset{o}{A}$). After r_{imp} becomes greater than 1.33 $\overset{o}{A}$, D drops unless more
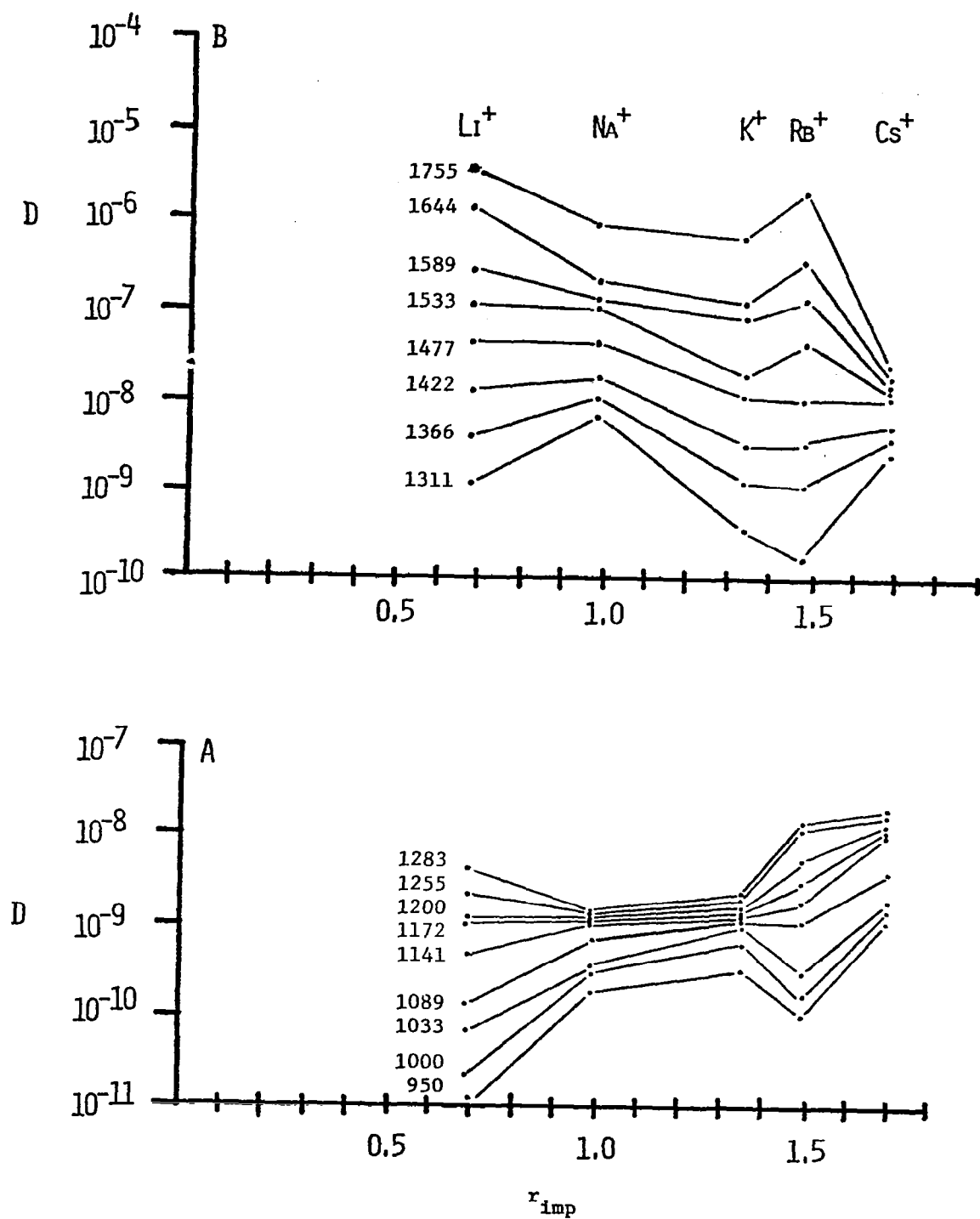
D(CM^2/SEC) VS r_{imp}(Å) AT CONSTANT T(°K) IN 304 STAINLESS STEEL

Figure 23

energy is given to increase the lattice vibrations. There appears to be a significant size effect at approximately 1.67 Å. The increase in D at lower temperatures is probably due to the fact that there are unit cells consisting of different sized lattice ions, so that larger ions than normal could diffuse through. However, this is a limited effect as T increases, the increased lattice vibrations no longer tend to increase D and the larger size of the impurity ion becomes a more dominant parameter.

In fact, there are two aspects to note. The first is that along with the other samples, as both r_{imp} and T increase it appears there may be an upper limit for impurity diffusion coefficients in these b.c.c. structures of approximately 10^{-8} cm^2/sec. The second is that as in the case of zircaloy-2, after the phase change the diffusion coefficient drops initially and then proceeds to rise with temperature.

As there are no reported values for the diffusion of the alkali metals in 304 stainless steel, it was thought that a comparison between Na-23 and C-14 diffusion in 304 and 316 stainless steel would be desirable. This would enable one to determine whether the results obtained via mass spectrometry were reasonable in comparison to the determination of diffusion coefficients by other methods for a different element. Table X illustrates that the Na-23 diffusion is within an order of magnitude of the diffusion of C-14. The Na-23 also seems to diffuse at a slower rate than the C-14 as would be expected since the Na-23 has a larger ionic radius than C-14. The C-14 diffusion coefficients were determined by Perkins and Carlson,[49]

Table X
C-14 & Na-23 Diffusion in 304 Stainless Steel

C-14 Diffusion			Na-23 Diffusion	
$T(^{\circ}K)$	D(ref 49)	D(ref.50)	$T(^{\circ}K)$	D(This Study)
873	$4.30 \cdot 10^{-10}$			
923	$1.81 \cdot 10^{-10}$	$4.27 \cdot 10^{-10}$		
943		$1.66 \cdot 10^{-10}$		
		$3.02 \cdot 10^{-10}$		
963				
973	$6.54 \cdot 10^{-10}$	$4.57 \cdot 10^{-10}$	948	$3.85 \cdot 10^{-10}$
993		$8.71 \cdot 10^{-10}$	983	$3.58 \cdot 10^{-10}$
1023		$1.91 \cdot 10^{-9}$	1002	$5.29 \cdot 10^{-10}$
1049	$3.36 \cdot 10^{-9}$		1044	$6.11 \cdot 10^{-10}$
1063				
1093		$3.98 \cdot 10^{-9}$		
		$7.25 \cdot 10^{-9}$		
1123	$9.54 \cdot 10^{-9}$	$1.02 \cdot 10^{-8}$	1106	$1.15 \cdot 10^{-9}$
			1122	$1.09 \cdot 10^{-9}$
1153		$2.19 \cdot 10^{-8}$	1133	$1.19 \cdot 10^{-9}$
			1149	$1.35 \cdot 10^{-9}$
1198		$4.36 \cdot 10^{-8}$	1168	$1.19 \cdot 10^{-9}$
1209	$2.83 \cdot 10^{-8}$		1208	$1.69 \cdot 10^{-9}$
1223		$6.61 \cdot 10^{-8}$		
			1227	$1.37 \cdot 10^{-9}$
			1239	$1.17 \cdot 10^{-9}$
			1241	$2.19 \cdot 10^{-9}$
1269	$9.74 \cdot 10^{-8}$			
1273		$1.45 \cdot 10^{-7}$		
			1276	$5.54 \cdot 10^{-9}$
1333			1326	$1.07 \cdot 10^{-8}$
1373		$2.75 \cdot 10^{-7}$		
1473		$5.01 \cdot 10^{-7}$		
		$1.54 \cdot 10^{-6}$		

and by Agarwala, Naik, Anand, and Paul.[50]

In the further analysis of the data, two additional relationships merit examination. Based on equation (48)

$$D = D_o \exp(-Q/RT)$$

it would seem that there should be some type of direct relationship between D_o and Q. Using the PDP 8/I computer a best fit least squares program was run utilizing data on D_o and Q for h.c.p., f.c.c., and b.c.c. structures and at all temperatures. It was found that the correlation coefficient for the best fit line was 0.98 where 1.0 is a perfect fit. Subsequently, it was determined that the relation between D_o and Q was

$$D_o = 3.3 \times 10^{-8} \exp\{(0.36)(Q)\} . \qquad (60)$$

Whether or not this equation applies only to a dilute solute diffusion of the alkali metals in these particular matrices, or for any other diffusing system requires further investigation.

A second interesting consequence of this work involves the possibility of using this method to further develop concepts on ultra-fast diffusion. Ultra-fast diffusion has been considered when the solute diffusion is much greater than self-diffusion in the host material. An example is the diffusion analysis of zircaloy-2 in this work. The self-diffusion rates of pure α-zirconium have been determined by Dyment and Libanati.[51] For a temperature range of 1036^oK to 1130^oK, they found D to be on the order of 10^{-12} to 10^{-13} cm^2/sec, while in this study, the diffusion rates of the alkali

metals for the same temperature range were on the order of 10^{-8} to 10^{-9} cm^2/sec. This is approximately four to five orders of magnitude faster. Ultra-fast diffusion has been suggested by Hood and Schultz[52] to take place by an interstitial mechanism. They studied both Co-60 and Fe-59 diffusion in pure α-zirconium and found that D was of the order of 10^{-7} to 10^{-9} cm^2/sec which corresponds well with this work. That ultra-fast diffusion would take place by an interstitial mechanism coincides with the mechanism for determining the largest diffusing ion size; a concept used to explain figures 22 and 23.

It should be further noted that in Part II, concepts of the jump frequency ω, the mean vibrational frequency, ν , and the change in free energy, ΔG, were all discussed. With the results obtained in this study, it now becomes important to determine some of these quantities.

Zener[39] has stated that while it would not be impossible for ΔG to increase with increasing temperature, it would be highly improbable. The reason for this is that a negative temperature coefficient of the elastic moduli exists. Zener also found that the change in entropy, ΔS can be related to the activation energy, Q, by

$$\Delta S = \lambda \beta Q / T_m \qquad (61)$$

where λ is a numerical coefficient essentially equal to

unity for interstitial, β is a dimensionless quantity tabulated by Zener for some pure metals, and T_m is the melting temperature for the host material. The value of ΔS can be used to calculate ν using

$$D_o = (1/6) \, a_o^2 \, \nu \, \exp \, (\Delta S/R) \qquad (62)$$

provided that D_o is known.

Of the three sample materials used in this study, β has been determined for tantalum only. It has a value of 0.40. Using values for D_o obtained experimentally, ν can be determined. Once the values of ν have been determined, ω can be calculated using equation (23).

$$\omega = \nu N_m = \nu \, \exp \, (-Q/RT) \, \exp \, (\Delta S/R)$$

Table XI gives the calculated values for ω for the five diffusing impurity isotopes in both temperature regimes.

Table XI

Calculated Values of ν and ω For Tantalum

$990 < T(^{\circ}K) < 1230$

Impurity	ν (sec^{-1})	exp(-Q/RT)	exp(ΔS/R)	ω (sec^{-1})
Li-7	2.83×10^{11}	.997	1.001	2.82×10^{11}
Na-23	1.14×10^{10}	.998	1.0007	1.13×10^{10}
K-39	1.49×10^{13}	.995	1.002	1.48×10^{13}
Rb-85	6.71×10^{14}	.994	1.002	6.68×10^{14}
Cs-133	4.69×10^{10}	.998	1.001	4.68×10^{10}

$1230 < T(^{\circ}K) < 1790$

Impurity	ν (sec^{-1})	exp(-Q/RT)	exp(ΔS/R)	ω (sec^{-1})
Li-7	1.86×10^{11}	.996	1.002	1.85×10^{11}
Na-23	6.22×10^{9}	.998	1.001	6.21×10^{9}
K-39	5.83×10^{10}	.997	1.001	5.82×10^{10}
Rb-85	1.28×10^{9}	.998	1.001	1.27×10^{9}
Cs-133	6.50×10^{9}	.998	1.001	6.49×10^{9}

Part VI

CONCLUSIONS

It was the purpose of this work to illustrate a new technique in the general field of materials characterization. The transport of impurities, in the p.p.m. to p.p.b. range and less, is becoming increasingly important. Since the mass spectrometer is an instrument which can detect impurity concentrations on this scale, it offers another view of the high temperature diffusion properties in materials which are of engineering usefulness. This is instead of being confined to the world of the single crystal.

As a consequence of this work, not only were the diffusion coefficients of the alkali metals in the sample materials calculated, but known phase transformations were determined in the samples of 304 stainless steel and zircaloy-2. This, of course, lends a measure of credibility to the results obtained.

While the primary intent of this work has been accomplished, it has been shown that what used to be a chemists tool can be applied in metallurgical research. It is not to be suggested that the mass spectrometer is the ultimate instrument, but rather that it allows one more unique way of looking at material's properties on the atomistic level. It is conceivable that by determining the relationship between the diffusion coefficient and the atomic radius of all the impurities in a material that a better understanding of diffusion processes could be obtained. It is hoped that

further funding will allow this laboratory to pursue this
and to see how ion implantation of selected species affect
the diffusion process in certain materials - i.e., semi-
conductors.

APPENDIX

Program to Determine Least Squares Fit of
Data to Exponential Curve, Correlation Coefficient,
and 95% Confidence Limit

C-8K FOCAL @1969

```
01.10 T !!,"THIS PROGRAM FITS PAIRS OF POINTS TO AN EXPONENTIAL
01.11 T !"LEAST SQUARES CURVE FIT - TO THE EQUATION: Y=A*EXP(B*X)
01.12 T !"    X IS THE RECTANGULAR ABSYSSA
01.13 T !"    Y IS THE RECTANGULAR ORDINATE (INTERNAL CONVERSION TO LOGY
01.14 T !"    A IS THE Y-INTERCEPT
01.15 T !"    B IS THE SLOPE ON SEMI-LOG PAPER
01.16 T !"    R IS THE CORRELATION COEFFICIENT
01.17 T !"    CL IS THE 95% CONFIDENCE LIMIT +/- AT X=(TEST POINT)
01.18 T !!"PROGRAM OPERATION:
01.19 T !"  AFTER FIRST PROMPT ENTER THE NUMBER OF ORDERED PAIRS
01.20 T !"    THEN  -ENTER X & Y AS REQUESTED BY THE PROGRAM
01.21 T !"          -ENTER T(0.025) FOR THE SPECIFIED D.F. WHEN REQUESTED
01.22 T !"          -ENTER THE NUMBER OF TEST POINTS
01.23 T !"          -ENTER THE TEST POINTS
01.30 A !!!"ENTER THE NUMBER OF VALUES: "N
01.35 S SX=0;S SY=0;S XT=0;S XY=0;S YT=0
01.40 I (N-1) 9.9,1.6
01.50 F I=1,N;D 2
01.55 G 3.1
01.60 T !"TRY AGAIN -- 1 IS NO GOOD
01.65 G 1.3

02.10 A !"ENTER X: "X,"ENTER Y: ",Y;S Y=FLOG(Y)
02.15 S SX=SX+X;S SY=SY+Y;S XT=XT+X↑2;S XY=XY+X*Y;S YT=YT+Y↑2

03.10 S X$=SX/N;S Y$=SY/N
03.15 T !!"THE AVERAGE VALUE OF X IS: ",%,X$
03.20 S YY=YT-(SY↑2/N)
03.30 S XX=XT-(SX↑2/N)
03.40 S TT=XY-(SY*SX/N)
03.50 S SS=(TT↑2)/XX
03.55 S MS=(YY-SS)/(N-2)
03.60 C CALCULATION OF THE SLOPE -- B
03.65 S B=TT/XX
03.70 C CALCULATION OF THE Y-INTERCEPT -- A
03.75 S A=FEXP(Y$-B*X$)
03.80 C CALCULATION OF THE CORRELATION COEFFICIENT -- R
03.85 S R=TT/FSQT(XX*YY)
03.90 G 5.10
```

```
04.10 C PRINT OUT THE RESULTS
04.20 T %,!!!"RESULTS:
04.30 T !"      THE SLOPE IS: ",B
04.40 T !"      THE Y-INTERCEPT IS: ",A
04.50 T !,"     THE CORRELATION COEFFICIENT IS: ",R
04.60 R
04.70 T !!!!"IF YOU WISH TO STOP -- AT THE NEXT PROMPT TYPE (-1)
04.80 T !"        OTHERWISE CONTINUE
04.90 G 1.3


05.10 C INPUT FOR THE DETERMINATION OF THE 95% C.L.'S FOR EACH TEST PT
05.15 T %2.0,!!"ENTER THE VALUE OF T(0.025) FOR ",N-2, " DEGREES
05.16 A " OF FREEDOM: ",DF
05.20 A !"ENTER THE NUMBER OF TEST POINTS: ",M
05.25 F I=1,M;D 6
05.30 DO 4
05.35 F I=1,M;S CL(I)=DF*FSGT(MS*(1/N+(X(I)-0)+2/XX))
05.36 F I=1,M;S Y(I)=FEXP(B*X(I))*A
05.37 F I=1,M;D 7
05.38 D 9.04
05.39 D 9.05
05.40 F I=1,M;D 9.1
05.45 G 4.70


06.05 C INPUT OF TEST POINTS -- X(M)
06.10 T %2.0,!"ENTER TEST POINT X(",I,"): "
06.20 A X(I)


07.10 S ZA=FEXP(FLOG(Y(I))+CL(I))
07.20 S ZB=FEXP(FLOG(Y(I))-CL(I))
07.30 S ZC(I)=FABS(ZA-ZB)/2


09.04 T !!"TEST POINTS AND THEIR RESPECTIVE 95% C.L.'S
09.05 T !!"  M              ","X(M)                    Y(M)                    CL"
09.10 T !,%2.0,I,%," ",X(I)," ",Y(I)," ",ZC(I)
09.90 T !"THE END";Q
*aaaaaaaaa
```

Program to Determine D for a Given Temperature
Provided D_o and Q are Supplied

```
C-8K FOCAL @ 1969

01.01 C PROGRAM: DIFF
01.02 C
01.10 A !!!"WHAT IS THE SAMPLE MATERIAL? ",A
01.20 A !"WHAT IS THE DIFFUSING ISOTOPE? ",A,B
01.30 A !"WHAT IS THE TEMPERATURE RANGE? ",A,"TO ",B,"DEGREES KELVIN."
01.35 A !"WHAT IS THE VALUE OF D(0)? "D0
01.40 A !"WHAT IS THE VALUE OF THE ACTIVATION ENERGY? "Q
01.60 T !,%

02.10 A !"T= ",T
02.15 I (T) 2.6,2.5
02.20 S D=D0*FEXP(-Q/(2E-3)*T)
02.25 G 3.1
02.30 T "          ","D= "D
02.31 G 2.1
02.35 T "          ","D= "D
02.40 G 2.1
02.50 G 1.1
02.60 T !!!!;Q

03.10 I (1000-T)2.3,2.3,2.35
*
```

REFERENCES

1. Fick, A., _Ann. Phy. Lpz._, 170, 59, 1855.

2. Fourier, J., _Theorie Analytique de Chaleur_,
   Oevures de Fourier, 1822.

3. Davidson, B., "Neutron Transport Theiry," Oxford
   University Press, London, p. 16, 1957.

4. Boltzmann, L., _Ann. Phys._, 53, 960, 1894.

5. Matano, C., _Japan. Phys._, 8, 109, 1938.

6. Gertsriken, S. D. and I. Y. Dekhtyar, "Solid State
   Diffusion in Metals and Alloys," AEC-tr-6313, USAEC
   Division of Technical Information, Washington, D. C.,
   1964.

7. Willard, N. H., L. L. Merritt, Jr., and J. A. Dean,
   "Instrumental Methods of Analysis," Fourth Edition,
   D. Van Nostrand, New York, p. 210, 1965.

8. McCracken, J. M. and H. M. Love, _Phys. Rev. Letters_,
   5, 201, 1960.

9. Walling, J. D., Doctor of Philosophy Thesis, R.P.I.,
   June, 1973.

10. Shewmon, P. G., "Diffusion in Solids," McGraw-Hill,
    New York, 1963.

11. Cottrell, A. H., "An Introduction to Metallurgy,"
    Edward Arnold Ltd., London, 1967.

12. Askill, John, "Tracer Diffusion Data for Metals, Alloys
    and Simple Oxides," IFI/Plenum Data Corp., New York,
    1970.

13. Shewmon, _op cit._, p. 7.

14. Walling, _op cit._, p. 35.

15. Compaan, K. and Y. Haven, _Trans. Faraday Soc._, 52,
    786, 1956.

16. Dekker, A. J., "Solid State Physics," Prentice-Hall,
    Englewood Cliffs, New Jersey, 1959.

17. Shewmon, _op cit._, p. 56.

18. Shewmon, _op cit._, p. 56.

19. Dekker, *op cit*., pgs. 65-67.

20. Dekker, *op cit*., p. 62

21. Zener, C., "Imperfections in Nearly Perfect Crystals," Wiley, New York, p. 287, 1952.

22. Dekker, *op cit*., p. 62.

23. Shewmon, *op cit*., p. 60.

24. Huntington, H. and P. Ghate, *Phys. Rev. Letters*, 8, 421, 1962.

25. Shewmon, *op cit*., p. 110.

26. Shewmon, *op cit*., p. 97.

27. Swalin, R., *Acta Met.*, 5, 443, 1951.

28. Overhauser, R. A., *Phys. Rev.*, 90, 393, 1953.

29. Reiss, H., *Phys. Rev.*, 113, 1445, 1959.

30. Feit, Michael; *Phys. Rev. B.*; 3, 1223, 1971.

31. Feit, Michael; *Phys. Rev. B*; 5, 2145, 1972.

32. Huntington, H. B., and F. Seitz; *Phys. Rev*; 61, 315, 1942.

33. Lazarus, David; *Phys. Rev*; 93, 973, 1954.

34. Johnson, R. P.; *Phys. Rev*; 56, 814, 1939.

35. Zener, C.; *Acta Cryst*; 3, 346, 1950.

36. LeClaire, A. D.; *Acta Metal*; 1, 438, 1953.

37. Wert, C. and C. Zener; *Phys. Rev*; 76, 1169, 1949.

38. Turnbull, D. and R. E. Hoffman; *Acta Metal.*; 7, 407, 1959.

39. Zener, C; *J. Applied Phys*; 22, 372, 1951.

40. White, F. A., and J. C. Sheffield, Knolls Atomic Power Laboratory Report, KAPL-873 (1952).

41. Schwegler, Jr., E. C., Doctor of Engineering Thesis, R.P.I., August 1967.

42. Langmuir, I. and K. H. Kingdon, *Proc. Roy. Soc. (London)*, A 197, pgs. 61-79, 1925.

43. Pande, B. M., M. C. Naik, and R. P. Agarwala, <u>J. of Nuc.</u> Mat., 28, 324, 1968.

44. Delong, W. T., <u>Welding Journel</u>, p. 274, July, 1974.

45. Son, R., M. Miyake, and T. Sano, <u>Tech. Rep. Osaka. Univ.</u>, 18, 317, 1968.

46. Zuchner, H., and E. Wicke, <u>Z. Phys. Chem. N.F.</u>, 67, 154, 1969.

47. Borisov, E. V., P. L. Gruzin and S. V. Zemskii, <u>Zosch.</u> <u>Pokvy. Metal.</u>, 2, 104, 1968.

48. Vandyshev, B. A. and A. S. Panoj, <u>Izv. Akad. Nauk, SSSR</u> <u>Metal</u>, 1, 244, 1969.

49. Perkins, R. A. and P. T. Carlson, <u>Metal. Trans.</u>, 5, 1511, 1974.

50. Agarwala, R. P., M. C. Naik, M. S. Anand, and A. R. Paul, <u>J. of Nuc. Mat.</u>, 36, 41, 1970.

51. Dyment, F. and C. M. Libanati, <u>J. of Mat. Sci.</u>, 3, 349, 1968.

52. Hood, G. M. and R. J. Schultz, Phil. Mag., 1972.

1. Report No. NASA CR-3165	2. Government Accession No.	3. Recipient's Catalog No.
4. Title and Subtitle DIFFUSION AND PHASE CHANGE CHARACTERIZATION BY MASS SPECTROMETRY		5. Report Date August 1979
		6. Performing Organization Code
7. Author(s) Mark E. Koslin and Frederick A. White		8. Performing Organization Report No.
		10. Work Unit No.
9. Performing Organization Name and Address Rensselaer Polytechnic Institute Troy, New York 12181		
		11. Contract or Grant No. NSG-1360
		13. Type of Report and Period Covered Contractor Report
12. Sponsoring Agency Name and Address National Aeronautics and Space Administration Washington, DC 20546		
		14. Sponsoring Agency Code

15. Supplementary Notes

Langley Technical Monitor: George M. Wood, Jr.

Final Report

16. Abstract

This report focuses on the high temperature diffusion of trace elements in metals and alloys. Specifically, these measurements have been made by high sensitivity mass spectrometry in which individual atoms were detected, and quantitative data was obtained for zircaloy-II, 304 stainless steel, and tantalum. Additionally, a mass spectrometer was also an analytical tool for determining an allotropic phase change for stainless steel at 955°C, and a phase transition region between 772°C and 1072°C existing for zircaloy-II.

Diffusion rates were measured in thin (0.001" (0.0025 cm) and 0.0005" (0.0013 cm)) ribbons which were designed as high temperature thermal ion sources, with the alkali metals as naturally occurring impurities. In the temperature and pressure regime where diffusion measurements were made, the solute atoms evaporated from the ribbon filaments when the impurities diffused to the surface, with a fraction of these impurity atoms ionized according to the Langmuir-Saha relation.

While these measurements were made on only a few important materials, the techniques developed can be clearly applied to many other alloys important to space vehicles and supersonic transports; and, with appropriate modifications, to the diffusion of impurities in composites.

17. Key Words (Suggested by Author(s)) Mass spectrometry Trace elements High temperature diffusion Crystallographic phase change	18. Distribution Statement Unclassified - Unlimited Subject Category 26
19. Security Classif. (of this report) Unclassified	20. Security Classif. (of this page) Unclassified	21. No. of Pages 108	22. Price* $6.50